Alma Mater Studiorum · University of Bologna

School of Science
Department of Physics and Astronomy
Master Degree in Physics

Entanglement entropy in the hopping and SSH model.

Supervisor:
Prof. Francesco Ravanini
Co-supervisor:
Prof. Benoit Estienne

Submitted by:
Andrea Gaspari

Academic Year 2021/2022

Abstract

Entanglement entropy is the core argument of this thesis. After a brief introduction of its properties and a review of the leading theoretical methods for its computation, it is studied in free fermion models, namely the hopping and the SSH model in one dimension. During this preliminary part, a code has been created to test numerically the main results. Reached a satisfactory level of reliability for this latter, simulations are used to probe second order symmetry resolved Rènyi entropies (SRRE) in the SSH model. This investigation is carried out considering both finite and infinite subsystems. In the second scenario, sharp patterns regarding the distribution of SRRE for different charge sectors are obtained and discussed. Supported by numerical data, exact formulae have been achieved to describe the outcomes. In the end, methods are rephrased to extend the analysis to more generic free fermion models.

Contents

Introduction

Physics at quantum level shows properties as fascinating as atypical. Unlike classical phenomena, a certain degree of uncertainty is in fact at the very core of quantum behaviour, along with quantization of energy levels, wave-particle duality and entanglement. Especially this latter is arguably the most controversial feature of the whole quantum framework as it violates the cardinal principle of causality. Introduced in 1935 by Dirac[1] and immediately questioned by Einstein, Podolsky and Rosen[2], entanglement can be intuitively described quoting one of Einstein's letter to Born[3] as a *"spooky action at distance"*. A statement unfolding clear discomfort towards a phenomenon in severe contrast with classical intuition.

It took almost three decades and the work of Bell[4] for entanglement to be undoubtedly recognized as an essential quantum property. Since then, it gained lot of attention from very different fields of research, ranging from black hole[5][6] to quantum information and computing[7][8] and quantum many-body theory[9]. Along with the rising awareness it came the need for a quantitative measure of entanglement which does not increase under local transformations and classical communications (LOCC). This urge led to the formulation of *entanglement monotones*[10] with many measures being proposed and finding use in the literature depending on the context[11]. For the purpose of this thesis I will investigate *entanglement entropy* (EE)[12].

Besides its simple definition, EE gained large popularity in recent years due to its multiple properties. For instance, in gapped systems it obeys an area law[13] while in one-dimensional systems, at criticality, it shows a logarithmic growth directly proportional to the *central charge* of the underlying theory[14], thus being able to spot quantum phase transitions. In systems with internal symmetry this measure can be further characterized for each charge sectors, hence taking the name of symmetry-resolved entanglement entropy SREE [15][16]. In this case, equipartition is expected between different sectors under precise conditions[17].

In the present work I studied EE in the hopping and SSH model. The initial part was devoted to the creation of a reliable code able to simulate numerically free fermionic chains and reproduce theoretical predictions regarding EE. By making use of it, I then probed entanglement equipartition in SSH model with exact computation of SREE.

Regarding the structure of the elaborate, Ch.(1) is meant to present the main theoretical elements and tools in order for the thesis to be self-consistent and let the reader get acquainted with the topic. In the second chapter(2) a detailed analysis of the models considered is provided with insights concerning the creation of the code that will serve

as useful resource for Ch.(3), where the problem of symmetry-resolved EE is tackled and the main results are discussed.

Chapter 1

Theoretical background

In this chapter an overview of the theoretical background of this thesis is provided. In order, an essential introduction with the main notions to describe entanglement measures, the correlation function method and, finally, the replica trick, are presented.

1.1 Entanglement measures

Far from being a complete introduction of such a vast and vivid topic[18], main axioms and properties of entanglement measures are reeled off for bi-partite systems, Fig.(1.1). The problem of defining and quantifying entanglement finds many possible answers depending on the field of research. From the quantum information point of view we are used to think at entanglement in a very operational way as a quantity due to quantum correlation that cannot be increased via local operations and classical communication (LOCC). In this framework entanglement measures were designed not only to give an answer whether a system is entangled or not, but to truly quantify how entangled a state is. To be consistent with the above premises a measure must then satisfy the following:

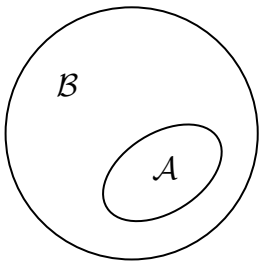

Fig. 1.1: Sketch of a bi-partition.

- *Entanglement must not increase due to LOCC,*
- *Separable states contain no entanglement,*
- *There exist maximally entangled states.*

Consider the case of a quantum system described by a pure state $|\psi\rangle$ and the bi-partition $\mathcal{A}$-$\mathcal{B}$. Assuming the Hilbert's space factorizes as $\mathcal{H} = \mathcal{H}_{\mathcal{A}} \otimes \mathcal{H}_{\mathcal{B}}$, one can write:

$$|\psi\rangle = \sum_{m,n} A_{mn} \, |\psi_m^{\mathcal{A}}\rangle \, |\psi_n^{\mathcal{B}}\rangle \, , \tag{1.1.1}$$

with the summation running over the elements of the bases $\{|\psi_m^{\mathcal{A}}\rangle\}$, $\{|\psi_m^{\mathcal{B}}\rangle\}$ of the two subsystems. Evidently, depending on the dimensions of $\mathcal{A}$ and $\mathcal{B}$, $A_{m,n}$ might not be a square matrix as one is not forced to take two equal-sized partitions. State $|\psi\rangle$ also admits

a singular value decomposition with Eq.(1.1.1) turning into:

$$|\psi\rangle = \sum_l \lambda_l \, |\phi_l^{\mathcal{A}}\rangle \, |\phi_l^{\mathcal{B}}\rangle \,, \tag{1.1.2}$$

with $\{|\phi_n^{\mathcal{A}}\rangle\}$, $\{|\phi_n^{\mathcal{B}}\rangle\}$ being two new orthonormal bases for the subsystems, coefficients λ_i real and positive definite and such that $\sum_l \lambda_l = 1$ if the state is normalized. This result goes under the name of *Schmidt decomposition*[19] and represents a very immediate tool to picture entanglement since coefficients λ_l encode all the information about it. With respect to these latter, a separable state is characterized by a single unitary coefficient $\lambda = 1$ while maximally entangled states are those for which all coefficients have the same value $\lambda_1 = \cdots = \lambda_D = \frac{1}{\sqrt{D}}$. Being able to recast $|\psi\rangle$ as in Eq.(1.1.2) might prove to be a hard task using singular value decomposition but it can be achieved using *density matrices*.

Starting from the full density matrix:

$$\rho = |\psi\rangle \, \langle\psi| \,, \tag{1.1.3}$$

one can define reduced density matrices (RDM) for bipartite systems, $\rho_{\mathcal{A}}$ and $\rho_{\mathcal{B}}$, tracing out the degrees of freedom of the complementary part of the system:

$$\begin{aligned} \rho_{\mathcal{A}} &= \mathrm{Tr}_{\mathcal{B}} \, \rho, \\ \rho_{\mathcal{B}} &= \mathrm{Tr}_{\mathcal{A}} \, \rho. \end{aligned} \tag{1.1.4}$$

Using Eq.(1.1.2), one can easily verify that their diagonal form must correspond to:

$$\rho_\alpha = \sum_l |\lambda_l|^2 \, |\phi_l^\alpha\rangle \, \langle\phi_l^\alpha| \,, \tag{1.1.5}$$

therefore, solving their eigenvalue problem automatically gives weights in Schmidt decomposition. For this reason their spectrum is also associated with the name of *entanglement spectrum*[20]. From Eq.(1.1.5) one can further realize the two RDM actually share the same spectrum, independently from their dimensions. Whereas entanglement spectrum allows to oultine the entanglement content we still lack the definition of a measure. Taking advantage of RDM let me thus introduce the *entanglement entropy*, defined as the Von Neumann entropy of ρ_α:

$$S_\alpha = -\,\mathrm{Tr}\, \rho_\alpha \ln \rho_\alpha, \tag{1.1.6}$$

which is none but the limit for $n \to 1$ of a larger class of EE going under the name of Rényi entropies:

$$S_{\alpha,\,n} = \frac{1}{1-n} \ln \mathrm{Tr}\, \rho_\alpha^n. \tag{1.1.7}$$

As it can be understood from its derivation, EE not only depends on quantum states but

also on the partition considered, yet, once it is fixed, there is no difference in considering one subsystem or its complementary as $S_{\mathcal{A}} = S_{\mathcal{B}} = S$. Coherently with the axioms presented before, it can be proven that EE is null for separable state and is maximal when all eigenvalues are identical. In this latter case $S = \ln D$.

As stated, many more measures enrich the framework but, in our case, Von Neumann and Rényi EE will be the ones considered and under observation for the rest of the elaborate.

1.2 Reduced density matrices and correlation function method

As anticipated in the above segment, to study and quantify entanglement, a key role is that of RDMs, yet deriving an explicit expression for them usually is a very demanding task, especially when many-body systems grow considerably in size. There are exceptions though. This is the case of free lattice models[21][22] and, in particular, of free-fermion chains[23]. The aim of this section is to revise the main steps for the computation of RDMs for these latter using correlation functions.

In the common sense, RDMs represent a basic tool of many-body theory in which they describe the properties of few selected particles out of the whole system. In our interest however, they acquire a slightly different connotation as they refer to a fixed subset of sites $\mathcal{A}$. In this framework consider the case of a partition given by a compact sequence of M sites as subsystem and a state described by a Slater determinant $|\psi\rangle$. For a generic free hamiltonian of the form:

$$\hat{H} = \frac{1}{2} \sum_{m,n} h_{m,n} c_m^\dagger c_n, \tag{1.2.1}$$

describing the system, all many-particle correlation functions factorize in products of two-point functions as a consequence of Wick's theorem[24] for free fermions. Readily:

$$\langle c_\alpha^\dagger c_\beta^\dagger c_\gamma c_\delta \rangle = \langle c_\alpha^\dagger c_\delta \rangle \langle c_\beta^\dagger c_\gamma \rangle - \langle c_\alpha^\dagger c_\gamma \rangle \langle c_\beta^\dagger c_\delta \rangle . \tag{1.2.2}$$

The set of all possible one-particle correlation functions thus encodes the whole theory content and it can be stored in a unique object constructing the so called *correlation function matrix* C, whose elements are defined as:

$$C_{m,n} = \langle c_m^\dagger c_n \rangle . \tag{1.2.3}$$

At this point, constraining the indexes to subsystem $\mathcal{A}$, id est $m, n \in \mathcal{A}$, one should recover the same result using the corresponding reduced density matrix $\rho_{\mathcal{A}}$, according to

the relation:

$$\langle c_i^\dagger c_j \rangle = \mathrm{Tr}(\rho_\mathcal{A} c_i^\dagger c_j), \qquad \textit{for: } i,j \in \mathcal{A}. \tag{1.2.4}$$

This is guaranteed again by Wick's theorem if $\rho_\mathcal{A}$ has the form of an exponential of a free-fermion operator:

$$\rho_\mathcal{A} = \frac{1}{Z} e^{-\hat{\mathcal{H}}} = \frac{1}{Z} \exp\Big[- \sum_{i,j\in\mathcal{A}} \tilde{h}_{i,j} c_i^\dagger c_j \Big], \tag{1.2.5}$$

with Z being a normalization constant. Here $\hat{\mathcal{H}}$ is usually known as the *entanglement hamiltonian* and must not be confused with the hamiltonian in Eq.(1.2.1) reduced to $\mathcal{A}$: $\hat{\mathcal{H}}$ is in fact an *ad-hoc* hamiltonian build to replicate the elements of C. Its explicit expression can be achieved considering its common diagonal representation with $C_\mathcal{A}$ and will allow us to determine the entanglement spectrum of the bipartition.

By being a density matrix, $\rho_\mathcal{A}$ must be hermitian and so does $\hat{\mathcal{H}}$ as a consequence, this implies the entanglement entropy always admits to be recasted in diagonal form:

$$\hat{\mathcal{H}} = \frac{1}{Z} \sum_p \epsilon_p \tilde{c}_p^\dagger \tilde{c}_p. \tag{1.2.6}$$

With respect to this new base $\{\tilde{c}_p\}$, normalization factor Z can be derived from the constraint $\mathrm{Tr}\,\rho_\mathcal{A} = 1$ as:

$$Z = \mathrm{Tr}(e^{-\hat{\mathcal{H}}}) = \sum_{\{k\}} \langle \{k\} |\, e^{-\sum_p \epsilon_p \tilde{n}_p} \,| \{k\} \rangle = \prod_p \sum_{\{k\}} \langle \{k\} |\, e^{-\epsilon_p \tilde{n}_p} \,| \{k\} \rangle = \prod_p (1 + e^{-\epsilon_p}). \tag{1.2.7}$$

Similarly, Eq.(1.2.4) becomes:

$$C_{ij} = \mathrm{Tr}(\rho_\mathcal{A} c_i^\dagger c_j) = \sum_{p,q} \Psi_p^*(i) \Psi_q(j)\, \mathrm{Tr}(\rho_\mathcal{A} \tilde{c}_p^\dagger \tilde{c}_q), \tag{1.2.8}$$

and focusing on $\mathrm{Tr}\,(\rho_\mathcal{A} \tilde{c}_p^\dagger \tilde{c}_q)$ with $\mathcal{H}_\mathcal{A}$ being free, one derives non-trivial results only for $p = q$, hence:

$$\begin{aligned}
\mathrm{Tr}\,(\rho_\mathcal{A} \tilde{n}_p) &= \sum_{\{k\}} \langle \{k\} | \frac{1}{Z} e^{-\sum_q \epsilon_q \tilde{n}_q} \tilde{n}_p | \{k\} \rangle = \sum_{\{k\}} \langle \{k\} | \frac{1}{Z} \frac{-\partial}{\partial \epsilon_p} e^{-\sum_q \epsilon_q \tilde{n}_q} | \{k\} \rangle = \\
&= \frac{1}{Z} \frac{-\partial}{\partial \epsilon_p} \sum_{\{k\}} \langle \{k\} | e^{-\sum_q \epsilon_q \tilde{n}_q} | \{k\} \rangle = -\frac{1}{Z} \frac{\partial}{\partial \epsilon_p} Z = -\frac{\partial}{\partial \epsilon_p} \ln \prod_k (1 + e^{-\epsilon_k}) = \\
&= -\frac{\partial}{\partial \epsilon_p} \Big[\sum_k \ln(1 + e^{-\epsilon_k}) \Big] = \frac{1}{e^{\epsilon_p} + 1}.
\end{aligned} \tag{1.2.9}$$

This latter equation unfolds the relations between the eigenvalues of the reduced correla-

tion matrix and the entanglement hamiltonian:

$$\xi_p = \frac{1}{e^{\epsilon_p}+1}, \tag{1.2.10}$$

$$\epsilon_p = \ln\frac{1-\xi_p}{\xi_p}, \tag{1.2.11}$$

moreover, using Eq.(1.2.11), $\rho_{\mathcal{A}}$ can be expressed explicitly as:

$$\begin{aligned}\rho_{\mathcal{A}} = \frac{e^{-\hat{\mathcal{H}}}}{Z} = \frac{\prod_p e^{-\epsilon_p \hat{n}_p}}{\prod_q (1-\xi_q)^{-1}} = \prod_p (1-\xi_p)\Big(\frac{\xi_p}{1-\xi_p}\Big)^{\hat{n}_p} = \\ = \otimes_{p\in\mathcal{A}}\Big[(1-\xi_p)\,|0\rangle_p\,\langle 0|_p + \xi_p\,|1\rangle_p\,\langle 1|_p\Big].\end{aligned} \tag{1.2.12}$$

From there, replacing it in Eq.(1.1.6), Von Neumann entropy simplifies as:

$$\begin{aligned}S_{\mathcal{A}} &= -\operatorname{Tr}\left[\frac{e^{-\sum_p \epsilon_p \tilde{n}_p}}{Z}\ln\frac{e^{-\sum_p \epsilon_p \tilde{n}_p}}{Z}\right] = -\operatorname{Tr}\Big[-\rho_{\mathcal{A}}\ln(Z) - \rho_{\mathcal{A}}\big(\sum_p \epsilon_p \tilde{n}_p\big)\Big] = \\ &= \langle\, \ln(Z) + \sum_p \epsilon_p \tilde{n}_p \,\rangle = \ln\Big[\prod_p (1-\xi_p)^{-1}\Big] + \sum_p \epsilon_p \xi_p = \\ &= -\sum_p \Big[\ln(1-\xi_p) - \epsilon_p\xi_p\Big] = -\sum_p \Big[\ln(1-\xi_p) - \xi_p \ln\Big(\frac{1-\xi_p}{\xi_p}\Big)\Big] = \\ &= -\sum_p \Big[(1-\xi_p)\ln(1-\xi_p) + \xi_p \ln(\xi_p)\Big].\end{aligned} \tag{1.2.13}$$

At this point it is interesting to note how eigenvalues ξ_p, as a direct consequence of their definition in Eq.(1.2.11), belong to the interval $[0,1]$, ensuring Von Neumann EE is well defined and always positive.

Code insights

Before proceeding to the next section let me quickly list and discuss some properties regarding C, $C_{\mathcal{A}}$ and their eigenvalues which have been useful during code writing as intermediate checks. Correlation function matrix C is such that it squares to itself, meaning $C^2 = C$ and all its eigenvalues must be either 0s or 1s; further, its trace matches the number of particles inside the subsystem. When the system is in a half-filled state, $C_{\mathcal{A}}$ also benefits of specific properties. In this case its trace corresponds to half the number of sites in the subsystem and it can be proven that its eigenvalues, if ordered by magnitude, satisfy the special relation[21][25]:

$$\xi_m = 1 - \xi_{M-m}. \tag{1.2.14}$$

1.3 Replica trick

Theoretical interest for EE is further enriched by its universal scaling in one dimensional systems at criticality. EE is in fact able to spot the location of quantum critical points and it is a quantity sensible to their most characterizing trait: the *central charge c* of the corresponding underlying theory. In numerical simulations these are extremely valuable information since entropies can be easily measured and they can be exploited to test the solidity of the code in use.

This preamble, although being very short, describes crucial predictions coming from the domain of *conformal field theories* which the reader might not be necessarily familiar with. As the title suggests, the main method involved is the so called *replica trick* which I will now illustrate and discuss in its main aspects. As this section will not cover the whole state of the art, for a more historical and complete description let me refer the works of *Calabrese & Cardy*[14][26][27] and the paper of *Holzhey, Larsen* and *Wilczek*[5].

Starting from the unitarity of the trace, $\sum_i w_i = 1$, and positive definiteness of RDMs, $w_i \geq 0$, eigenvalues w_i must lie in the interval $[0, 1]$. The sum $\operatorname{Tr} \rho_{\mathcal{A}}^n = \sum_i w_i^n$ is thus absolutely convergent for any $n > 1$ and therefore analytical. This remains true even promoting n to a real variable as long as it is bigger than one. At this point, if the entropy $S_{\mathcal{A}} = -\sum_i w_i \ln w_i$ is finite, we can capitalize $n \in \mathbb{R}$ and rephrase Von Neumann entropy as:

$$S_{\mathcal{A}} = -\lim_{n\to 1} \frac{\partial}{\partial n} \operatorname{Tr} \rho_{\mathcal{A}}^n = \lim_{n\to 1} S_{\mathcal{A},\, n}. \tag{1.3.1}$$

Here is where replica trick comes into play. Being able to determine $\operatorname{Tr} \rho_{\mathcal{A}}^n$ is, in fact, a difficult task generally but considering the analytical continuation of n, the problem reduces to the computation of a partition function on a specific *Riemann surface*, which is achievable using tools of *quantum field theories*. To be able to understand it however, few intermediate concepts must be introduced.

1.3.1 Path integral formulation of reduced density matrices

Consider a well-defined lattice quantum theory in $1 + 1$ dimension with continuous time. Lattice sites are labelled by a discrete variable x whose domain can be finite, semi-infinite or infinite. A complete set of observable is defined by $\{\hat{\phi}_x\}$ with corresponding eigenvalues and eigenstates represented respectively by $\{\phi_x\}$ and $|\{\phi_x\}\rangle$. A generic state $|\psi\rangle$ for the system is then given by a linear combination of $\otimes_x |\{\phi_x\}\rangle = |\prod_x \{\phi_x\}\rangle$, which indeed constitute a basis. Assuming the dynamics is ruled by the hamiltonian H and recalling Eq.(1.2.5), one might note a similitude between ρ and the quantum time operator e^{-itH}, especially if we move to an imaginary time $t \to -i\beta$. This analogy is indeed very meaningful as it allows to rephrase density matrices using path integral formalism. In details,

elements of ρ in a thermal state at inverse temperature β are given by:

$$\rho(\phi|\phi') \equiv \langle \prod_x \{\phi_x\}| \, \rho \, |\prod_{x'} \{\phi'_{x'}\}\rangle = \langle \prod_x \{\phi_x\}| \, \frac{e^{-\beta H}}{Z(\beta)} \, |\prod_{x'} \{\phi'_{x'}\}\rangle \,, \tag{1.3.2}$$

with $Z(\beta) = \mathrm{Tr}(e^{-\beta H})$ being the partition function. The same expression can be in fact interpreted as the path integral for the imaginary time interval $[0, \beta]$:

$$\rho(\phi|\phi') = \frac{1}{Z} \int [d\phi(y,\tau)] \prod_{x'} \delta(\phi(y,0) - \phi'_{x'}) \prod_x \delta(\phi(y,\beta) - \phi_x) e^{-S_E}, \tag{1.3.3}$$

with $S_E = \int_0^\beta d\tau L$ being the euclidean action and L the euclidean lagrangian. In the interest of clarity Eq.(1.3.3) is usually juxtaposed with its graphic counterpart. As can be observed in Fig.(1.2), the path integral version of ρ can be imagined as the evolution of the initial field, represented as a line on the x-axis, toward the final configuration with time on the y-axis. Accordingly, the partition function $Z = \mathrm{Tr}\,\rho$ is found setting $\phi = \phi'$, which has the effect of gluing together the two edges, forming a cylinder of circumference β. Reasonably, in the limit for $\beta \to \infty$ the cylinder becomes a plane.

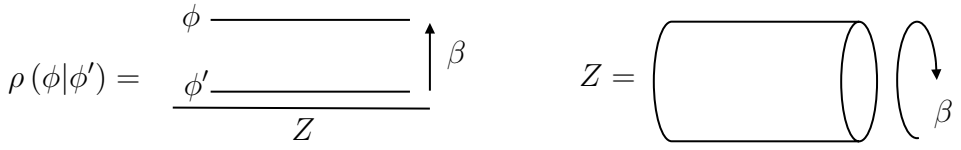

(a) Path integral of $\rho(\phi|\phi')$. (b) Partition function Z.

Fig. 1.2: Path integral visualization of density matrices. On the left the generic element $\rho(\phi|\phi')$ is pictured. On the right the partition function is obtained for $\phi = \phi'$, hence gluing the edges in (a). The circumference of the final cylinder is equal to β.

Chosen a subsystem $\mathcal{A}$ consisting of a compact set of points, $\mathcal{A} = [u, v]$, the corresponding reduced density matrix $\rho_\mathcal{A}$ is obtained form Eq.(1.3.3) gluing together all the sites not included in $\mathcal{A}$, thus leaving a cut open in the cylinder, Fig.(1.3). In principle nothing forbids to take more exotic subsystems, for instance considering disjoint intervals of points, but in practice this cause the rest of the procedure to be way more complicated, sometimes not even solvable at the present stage. For the purposes of my thesis then, only compact intervals are discussed.

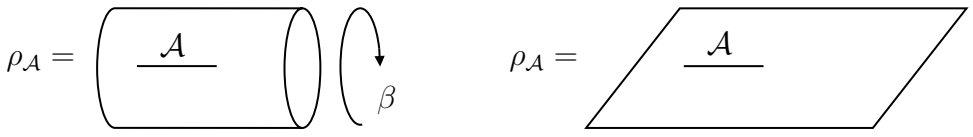

(a) $\rho_\mathcal{A}$ for finite time β. (b) $\rho_\mathcal{A}$ for infinite time $\beta \to \infty$.

Fig. 1.3: Path integral of $\rho_\mathcal{A}$.

1.3.2 Replicated target space and twist fields

Given the definition of $\rho_{\mathcal{A}}$, the computation of $\mathrm{Tr}\,\rho_{\mathcal{A}}^n$ is secured by making n copies of the above structures, for n being any positive integer, and gluing them together imposing the appropriate continuity equations:

$$\begin{aligned}\phi_j(x,\tau=\beta^-) &= \phi_{j+1}(x,\tau=0^+),\\ \phi_n(x,\tau=\beta^-) &= \phi_1(x,\tau=0^+).\end{aligned} \tag{1.3.4}$$

This procedure defines an *n-sheeted Riemann surface*. In Fig.(1.4) it is pictured for $n=3$ and β both finite and infinite. Partition functions on these surfaces are denoted by $Z_n(\mathcal{A})$ and are such that:

$$\mathrm{Tr}\,\rho_{\mathcal{A}}^n = \frac{Z_n(\mathcal{A})}{Z^n}, \tag{1.3.5}$$

which allow to solve Eq.(1.3.1).

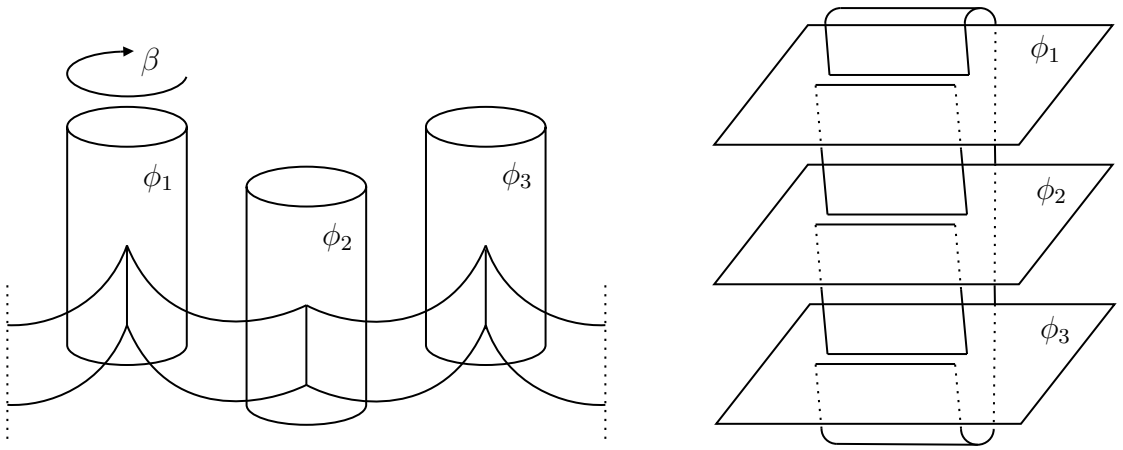

(a) 3-*sheeted Riemann surface* for finite β.

(b) 3-*sheeted Riemann surface* for β infinite.

Fig. 1.4: Pictures of 3-*sheeted Riemann surfaces* for a single compact interval $\mathcal{A}$.

Identified an *n-sheeted Riemann surface* with $\mathcal{R}_n$, the corresponding partition function $Z_n(\mathcal{A})$ can be expressed as:

$$Z_n(\mathcal{A}) = \int [d\phi]_{\mathcal{R}_n} e^{-\int_{\mathcal{R}_n} dx d\tau \mathcal{L}[\phi]}, \tag{1.3.6}$$

with $\mathcal{L}[\phi]$ being the local lagrangian density. At this point, since the only points with non-trivial effects of $\mathcal{R}_n$ are those located at the boundaries of $\mathcal{A}$, we are expected to be allowed to rephrase $Z_n(\mathcal{A})$ in terms of the action of abstract *fields* in u and v for a theory defined on the complex plane $z = x + i\tau$ with proper boundary conditions. Such fields are indeed defined by the above equation which encodes their correlation functions. Still, extracting them directly from Eq.(1.3.6) would result in the formulation of non-local

fields[28], which is something we generally prefer to avoid in physics. To recover local fields it is first necessary to re-adapt the topology of the *Riemann surface* to the target space where they are defined. This is done considering a model formed by n independent copies of the original one so the partition function in Eq.(1.3.6) can be rewritten as:

$$Z_n(\mathcal{A}) = \int_{[u,v]} [d\phi_1 \cdots d\phi_n] e^{-\int_{\mathbb{C}} dx d\tau (\mathcal{L}[\phi_1] + \cdots + \mathcal{L}[\phi_n])}. \tag{1.3.7}$$

The integration over $[u, v]$ now indicates the restricted path integral with conditions:

$$\phi_i(x, 0^+) = \phi_{i+1}(x, 0^-) \quad \textit{for: } x \in [u, v], \tag{1.3.8}$$

and we might introduce the Lagrangian density of the multi-copy model defined as:

$$\mathcal{L}^{(n)}[\phi_1 \cdots \phi_n](x, \tau) = \mathcal{L}[\phi_1](x, \tau) + \cdots + \mathcal{L}[\phi_n](x, \tau). \tag{1.3.9}$$

Fields described by Eq.(1.3.7) are now local and are associated to two opposite operations schematized in Fig.(1.5):

$$\mathcal{T}_n : \quad \phi_i(x) \mapsto \phi_{i+1}(x), \tag{1.3.10}$$

$$\tilde{\mathcal{T}}_n : \quad \phi_{i+1}(x) \mapsto \phi_i(x), \tag{1.3.11}$$

with the latter essentially coinciding to the inverse of the former.

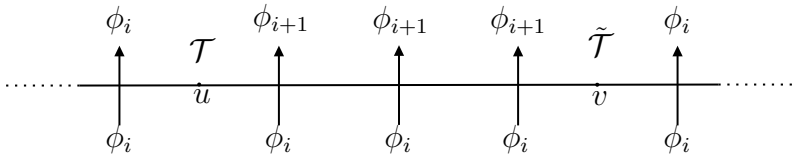

Fig. 1.5: Scheme of twist fields action.

They are called *branch-point twist fields* and are such that the partition function on the *n-sheeted Riemann surface* is proportional to their propagator in a replicated theory:

$$Z_n(\mathcal{A}) \propto \langle \mathcal{T}_n(u) \tilde{\mathcal{T}}_n(v) \rangle_{\mathcal{L}^{(n)}, \mathbb{C}}. \tag{1.3.12}$$

More in general, this identification holds for correlation functions in $\mathcal{R}_n$ as:

$$\langle \phi(x, \tau, \text{sheet } j) \cdots \rangle_{\mathcal{L}, \mathcal{R}_n} = \frac{\langle \mathcal{T}_n(u_1, 0) \tilde{\mathcal{T}}_n(v_1, 0) \phi_j(x, \tau) \cdots \rangle_{\mathcal{L}^{(n)}, \mathbb{C}}}{\langle \mathcal{T}_n(u_1, 0) \tilde{\mathcal{T}}_n(v_1, 0) \rangle_{\mathcal{L}^{(n)}, \mathbb{C}}}, \tag{1.3.13}$$

with ϕ_j fields in the model $\mathcal{L}^{(n)}$ coming from the j^{th} copy of $\mathcal{L}$.

1.3.3 Von Neumann entropy in an infinite chain

In the interest of clarity this section contains a detailed analysis to derive the main formulae. The example of an infinite chain is accompanied with explicit calculations.

Consider the case of a single interval $[u, v]$ of length $M = |u - v|$ in an infinitely long one-dimensional chain at zero temperature. Complex coordinates are here obtained from $\mathcal{R}_n$ after a double transformation. In the first place it is necessary to map the branch cut $[u, v]$ to the real axis, secondly, all Riemann surfaces must be squeezed in a unique plane. Explicitly, one has, starting from $w = x + i\tau$:

$$w = x + i\tau \;\; \rightarrow \;\; \zeta = \frac{w-u}{w-v} \;\; \rightarrow \;\; z = \zeta^{\frac{1}{n}}. \tag{1.3.14}$$

For a better understanding, the scheme can be observed in Fig.(1.6) where branch cuts are represented by wavy lines.

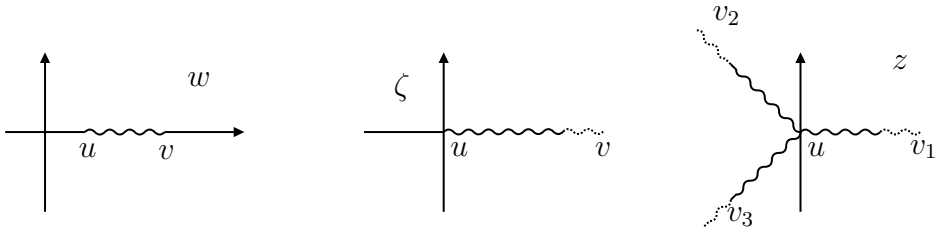

Fig. 1.6: Scheme to map $\mathcal{R}_3$ in $\mathbb{C}$. Wavy lines represent branch cuts: in a 3-*sheeted Riemann surface* we have three planes glued together which in the last step are squeeze in $\mathbb{C}$.

At this point, we consider the holomorphic component of the stress-energy tensor $T(w)$ which, under conformal transformations, is related to $T(z)$ according to[29]:

$$T(w) = \left(\frac{dz}{dw}\right)^2 T(z) + \frac{c}{12}\{z, w\}, \tag{1.3.15}$$

with $\{z, w\}$ being the Schwartzian derivative. Once there, knowing $\langle T(z)\rangle_{\mathbb{C}}$ must be zero to preserve symmetries, one may write:

$$\langle T(w)\rangle_{\mathcal{R}_n} = \frac{c}{24}\left(1 - \frac{1}{n^2}\right)\frac{(u-v)^2}{(w-u)^2(w-v)^2}, \tag{1.3.16}$$

which, however, corresponds to the expectation value of just a single copy of T and must be then multiplied for n to find $\langle T^{(\mathrm{tot})}\rangle$. Finally, recalling Eq.(1.3.13) and comparing it with the *conformal Ward identity*[30]:

$$\frac{\langle T(z)\phi(z_1)\phi(z_2)\rangle}{\langle \phi(z_1)\phi(z_2)\rangle} = \Delta\frac{(z_1 - z_2)^2}{(z - z_1)^2(z - z_2)^2} \tag{1.3.17}$$

everything boils down to:

$$\Delta = \frac{c}{24}\Big(n - \frac{1}{n}\Big), \tag{1.3.18}$$

which is half of the conformal scaling dimension of our twist fields. Indeed it can be proven $\Delta = \bar{\Delta}$. Twist fields thus act as primary fields under conformal transformations and their two-point function follows the usual rule:

$$\langle \mathcal{T}_n(u)\bar{\mathcal{T}}_n(v)\rangle \propto |u-v|^{-4\Delta}. \tag{1.3.19}$$

Replacing this result in Eq.(1.3.12) drive us to the explicit relation:

$$Z_n(\mathcal{A}) = \operatorname{Tr}\rho_{\mathcal{A}}^n = c_n\, M^{-\frac{c}{6}(n-\frac{1}{n})}, \tag{1.3.20}$$

where c_n is a constant and should not be confused with the central charge c.

Ultimately, taking the analytical continuation for n non-integer, the derivative in Eq.(1.3.1) can be solved, leaving us with the final result:

$$S_{\mathcal{A}} = \frac{c}{3}\ln M + c_1'. \tag{1.3.21}$$

Changing slightly the initial setup and moving to the case of a finite one-dimensional chain at criticality, the whole machinery is still effective but needs few adjustments. Specifically, assuming a system of size L, the RDM $\rho_{\mathcal{A}}$ at zero-temperature takes the form of a cylinder with L as circumference. When mapping the *Riemann surface* to the complex plane it is thus necessary to stretch the cylinder into a plane firstly and subsequently one can apply the scheme in Eq.(1.3.14). The former step is achieved using a complex exponential with initial coordinates $y = \tau + ix$ going to $w = e^{\frac{2\pi y}{L}}$. Propagating the variation in successive steps leads us to:

$$S_{\mathcal{A}} = \frac{c}{3}\ln\left(\frac{L}{\pi}\sin\frac{\pi M}{L}\right) + c_1'. \tag{1.3.22}$$

Coherently, in the limit for the chain growing indefinitely, $L \to \infty$, Eq.(1.3.22) replicates Eq.(1.3.21). These latter formulae are of major importance for this work as they will serve to both check the value of the central charge is correct and verify if numerical simulations match the predictions.

In general, whenever the topology of the *Riemann surface* is equivalent to those in Fig.(1.4), the problem can be addressed following the above procedure. Nonetheless, for the purposes of my thesis I won't discuss further examples as Eqs.(1.3.21), (1.3.22) already fulfill my needs.

Chapter 2

Analysis of free fermionic chains

In this chapter the hopping and the SSH models are studied. Starting with a brief overview of the two, the attention is mostly drawn to describe their entanglement content.

2.1 Hopping model

Hopping models are a family of models describing systems whose dynamics is characterized by *discretized kinetics terms*. This is the case, for example, of particles in discrete lattices. They might present different ranges of hopping, different amplitudes and, sometimes, even interactions and potentials are included. In the following sections I will consider arguably the simplest among them with jumps being described by a unique hopping parameter and occurring only between first neighbors in one-dimension. The analysis will treat both the finite and infinite chain scenarios.

2.1.1 Finite dimensional chain

The hopping model for first neighbours with a single hopping parameters t is described by the hamiltonian $\hat{H}$:

$$\hat{H} = -t \sum_{n=0}^{N-1} \Big(|n\rangle \langle n+1| + |n+1\rangle \langle n| \Big), \tag{2.1.1}$$

or, in second quantization formalism:

$$\hat{H} = -t \sum_{n=0}^{N-1} \Big(c_n^\dagger c_{n+1} + c_{n+1}^\dagger c_n \Big). \tag{2.1.2}$$

It describes the dynamics of fermions on a chain without the presence of any potential or interaction and, precisely for this latter detail, $\hat{H}$ can be addressed either as a single-particle or a many-body hamiltonian. N is a finite integer and corresponds to the total number of sites in the chain. Embedding the system on a ring, corresponding to the introduction of *periodic boundary condition* for which we identify the sites n and $n+N$, $\hat{H}$ commutes with the translational operator $\hat{T}$:

$$\hat{T} = \sum_m |m+1\rangle \langle m| , \quad \textit{such that:} \;\; [\hat{H}, \hat{T}] = 0. \tag{2.1.3}$$

$\hat{H}$ thus admits block-diagonal form. Such simplified version can be derived introducing plane waves, id est moving to momentum space. Eigenstates are then given by the discrete Fourier transforms:

$$|k(q)\rangle = \frac{1}{\sqrt{N}} \sum_{n=0}^{N-1} e^{ik(q)n} |n\rangle , \tag{2.1.4}$$

for $k = \frac{2\pi}{N} \cdot q$, $q \in [0, N-1]$ and the prefactor $\frac{1}{\sqrt{N}}$ in front to grant normalization. The set $\{|k(q)\rangle\}_{q=0,\dots,N-1}$ hence forms an orthonormal basis for the system. For completeness, inverse transformations are eventually given by:

$$|n\rangle = \frac{1}{\sqrt{N}} \sum_{q=0}^{N-1} e^{-ik(q)n} |k(q)\rangle . \tag{2.1.5}$$

Employing the lexical from solid state physics[31], one usually refers to $k(q)$ as *wavevector* and it either spans from $[0, 2\pi[$ or $[-\pi, \pi[$ depending on the domain of the quantum number q: $q \in [0, N[$ in the former case, $q \in [-\frac{N}{2}, \frac{N}{2}[$ in the latter. Wavevectors $k(q)$ are fundamental to study the energy spectrum as they identify a so called *Brilloiun zone*, where all quantum energy states are hosted.

Taking advantage of Eq.(2.1.5), $\hat{H}$ can be rephrased in momentum space, where it is completely diagonal:

$$\begin{aligned}
\hat{H} &= -t \sum_{n=0}^{N-1} \Big(|n\rangle \langle n+1| + |n+1\rangle \langle n| \Big) = \\
&= -\frac{t}{N} \sum_{n,q,p=0}^{N-1} \Big(e^{ik(p)} e^{-i[k(q)-k(p)]n} |k(q)\rangle \langle k(p)| + e^{-ik(q)} e^{-i[k(q)-k(p)]n} |k(q)\rangle \langle k(p)| \Big) = \\
&= -t \sum_{q=0}^{N-1} \Big(e^{ik(q)} + e^{-ik(q)} \Big) |k(q)\rangle \langle k(q)| = \\
&= \sum_{q=0}^{N-1} -2t \cos[k(q)] |k(q)\rangle \langle k(q)| \equiv \begin{pmatrix} \hat{\tilde{H}}_{q=0} & \cdots & 0 \\ \vdots & \ddots & \vdots \\ 0 & \cdots & \hat{\tilde{H}}_{q=N-1} \end{pmatrix} .
\end{aligned} \tag{2.1.6}$$

Once here, fixing the value of the hopping parameter t in this latter expression allows us to completely outline the energy spectrum. Few examples are provided in Fig.(2.1) in which two essential features can be easily noted. *In primis*, the spectrum becoming finer and finer the more sites the chain hosts. *In secundis*, the presence of null-energy states for $q = \frac{N}{4}$ when N is indeed a multiple of 4.

Knowing the spectrum, let me define the *groundstate* of the system as the zero temperature filled Fermi's sea, id est, the state with all negative eigenstates occupied. Using

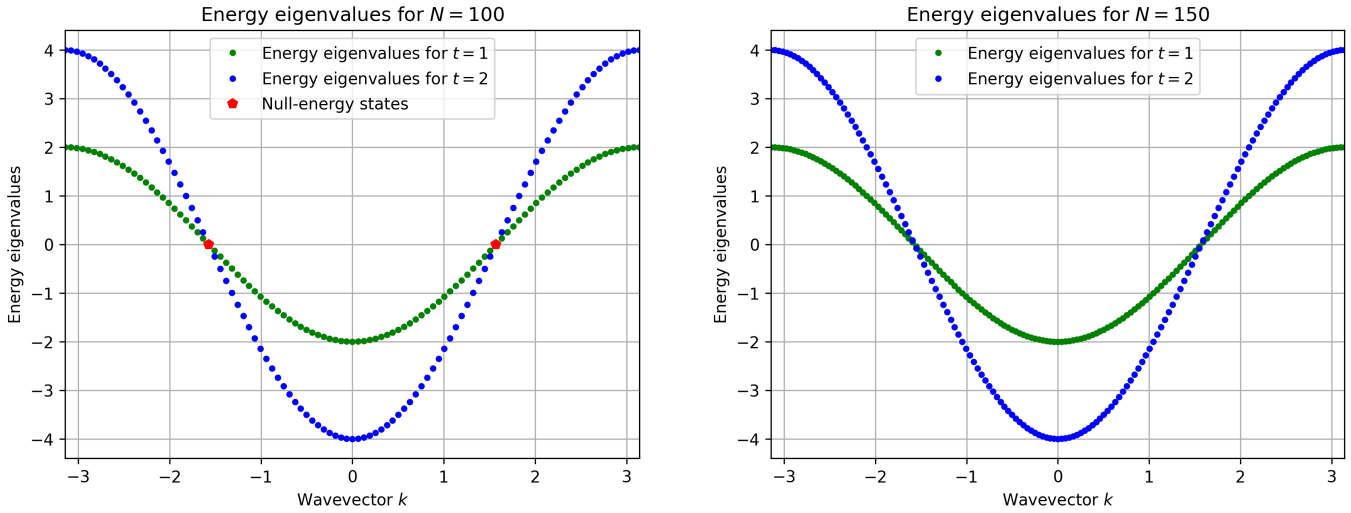

(a) Spectrum for $N = 100$.

(b) Spectrum for $N = 150$.

Fig. 2.1: Spectra for two different values of the hopping parameter $t = 1, 2$ in a chain of: **a)** $N = 100$, **b)**$N = 150$.

ladder operators of momentum space it can be expressed as:

$$|gs\rangle = \prod_{|q|\leq q_F} \tilde{c}_q^\dagger |0\rangle \,, \tag{2.1.7}$$

with $q_F = \frac{N}{4}$ being the quantum number fixing the Fermi level. Clearly this is a many-body state since the chain is half-filled. At this point it is interesting to note the effects of null-energy states which cause the groundstate to be degenerate. As a consequence, the summation for $|q| \leq q_F$ might be improperly defined as states related to q_F can be either included or not in $|gs\rangle$ without changes in the total energy. During simulations, to avoid any possible subtlety, a practical solution is to examine only systems with N not divisible by 4: this way the summation immediately restricts to $|q| < q_F$ as no states related to q_F are present. With respect to Eq.(2.1.7) and tracing back the steps in Sec.(1.2), the elements of C in the hopping model read as:

$$\begin{aligned} C_{mn} = \langle gs|c_m^\dagger c_n|gs\rangle &= \frac{1}{N}\langle gs| \left[\sum_{q=-N/2}^{N/2} e^{-ik(q)m}\tilde{c}_q^\dagger\right]\left[\sum_{p=-N/2}^{N/2} e^{ik(p)n}\tilde{c}_p\right]|gs\rangle = \\ &= \frac{1}{N}\sum_{q,p=-N/2}^{N/2} e^{-i[k(q)m-k(p)n]}\langle gs|\tilde{c}_q^\dagger\tilde{c}_p|gs\rangle = \\ &= \frac{1}{N}\sum_{|q|<q_F} e^{-ik(q)(m-n)}. \end{aligned} \tag{2.1.8}$$

From there, indicating with $\bar{q}$ the extremes for q, such that $|q| < q_F \to q \in [-\bar{q}, \bar{q}]$, one

can further manipulate the result as follows:

$$\begin{aligned} C_{mn} &= \frac{1}{N}\sum_{q=-\bar{q}}^{\bar{q}} e^{-ik(q)(m-n)} = \frac{1}{N}\sum_{q=-\bar{q}}^{\bar{q}} e^{-i\frac{2\pi}{N}(m-n)q} = \frac{1}{N}\sum_{q=-\bar{q}}^{\bar{q}} b^q = \\ &= \frac{b^{-\bar{q}}}{N}\sum_{q=0}^{2\bar{q}} b^q\Big(\frac{1-b}{1-b}\Big) = \frac{b^{-\bar{q}}}{N(1-b)}(1-b^{2\bar{q}+1}) = \\ &= \frac{b^{\frac{1}{2}}}{Nb^{\frac{1}{2}}}\frac{b^{-(\bar{q}+\frac{1}{2})}-b^{+(\bar{q}+\frac{1}{2})}}{b^{-\frac{1}{2}}-b^{\frac{1}{2}}} = \frac{1}{N}\frac{e^{i\frac{2\pi}{N}(m-n)(\bar{q}+\frac{1}{2})}-e^{-i\frac{2\pi}{N}(m-n)(\bar{q}+\frac{1}{2})}}{e^{i\frac{2\pi}{2N}(m-n)}-e^{-i\frac{2\pi}{2N}(m-n)}} = \\ &= \frac{1}{N}\frac{\sin\left[k(\bar{q})(m-n)+\frac{\pi}{N}(m-n)\right]}{\sin\left[\frac{\pi}{N}(m-n)\right]}. \end{aligned} \tag{2.1.9}$$

Note that for $m = n$ this expansion would be undefined. For this trivial case however it is enough to consider the initial formula (2.1.8) as it becomes:

$$C_{mm} = \frac{1}{N}\sum_{q=-\bar{q}}^{\bar{q}} 1 = \frac{1}{2}, \tag{2.1.10}$$

at least as long as we consider a chain with an even number of sites. At this point, selected a compact subsystem $\mathcal{A}$ as in Fig.(2.2), which can be thought as the set of consecutive sites $\mathcal{A} = [i, i+M]$ with M being its size, we aim to define $\rho_{\mathcal{A}}$. We thus reduce the correlation matrix C to $C_{\mathcal{A}}$, discarding all the terms involving sites not belonging to the subsystem:

$$C = \begin{pmatrix} C_{1,1} & \cdots & C_{1,N} \\ \vdots & \ddots & \vdots \\ C_{N,1} & \cdots & C_{N,N} \end{pmatrix} \rightsquigarrow C_{\mathcal{A}} = \begin{pmatrix} C_{i,i} & \cdots & C_{i,i+M} \\ \vdots & \ddots & \vdots \\ C_{i+M,i} & \cdots & C_{i+M,i+M} \end{pmatrix}$$

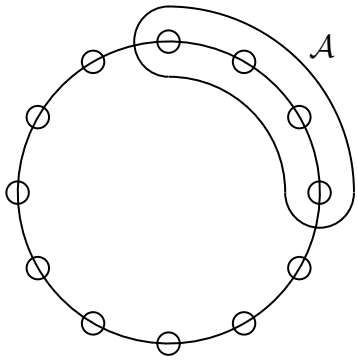

Fig. 2.2: Sketch of a compact subsystem $\mathcal{A}$ for a hopping model on a ring.

and then numerically compute its eigenvalues. In Fig.(2.3(a)) an example of entanglement spectrum for a subsystem of size $M = 30$ is provided. As it can be noticed, eigenvalues are no longer just zeros and ones but they still have the tendency of staying close to those extremes. This is a consequence of the introduction of boundaries and the formation of edge states while the bulk remain unchanged.

Finally, all unknown variables in Eqs.(1.2.12), (1.2.13) have been found so one can determine the reduced density matrix and entanglement entropy of subsystem $\mathcal{A}$. A plot for this latter can be observed in Fig.(2.3(b)) for different sizes M of the subsystem. What emerges is the graph of a reversed parabola showing a maximum when M corresponds precisely to half the size of the chain. Over numerical results a fit has been performed using the equation for Von Neumann entropy predicted by CFT, Eq.(1.3.22), which allowed us to determine the two parameters $c = 1$ and $c_1' = 0.73$. These results agree with the expected values[27] with the former telling us that we are studying Dirac's fermions.

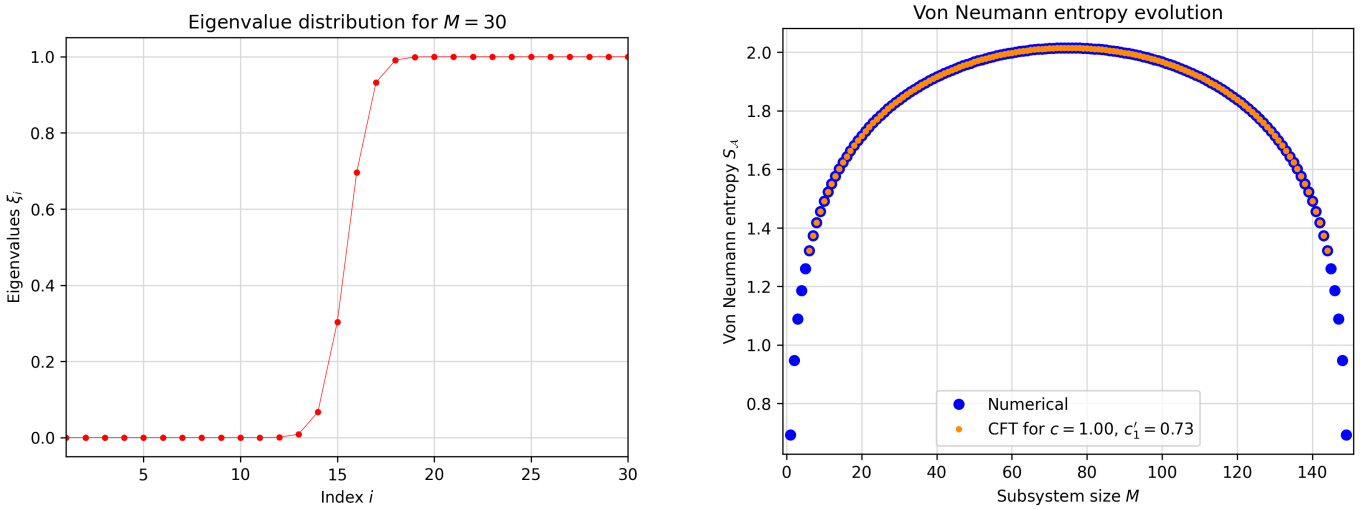

(a) Eigenvalue spectrum for $M = 30$.

(b) Von Neumann entropy for variable sizes.

Fig. 2.3: a) Eigenvalue distribution for a subsystem of size $M = 30$ on a ring of size $N = 150$, **b)** Von Neumann entropies comparison from a numerical and a CFT approach.

2.1.2 Infinite dimensional chain

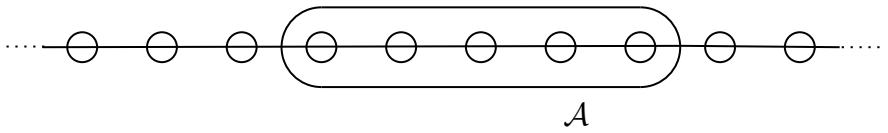

Fig. 2.4: Sketch of a subsystem in the infinite chain.

Extending the analysis to an infinite chain is straightforward but it needs the proper expedients. First of all, as one might expect from what claimed beforehand about energy eigenvalues getting denser and denser, in this case the system develops a continuous energy band as it can be observed in Fig.(2.5). Thereafter, defined once more the groundstate as a filled Fermi sea, the goal is to derive C. Nonetheless, for an infinite chain, this would be an impossible task as C would be an infinite dimensional matrix. Taking a look back, one might realize this is not really necessary as to define the reduced density matrix $\rho_{\mathcal{A}}$ the correlation function method, in reality, only makes use of $C_{\mathcal{A}}$. Thus,

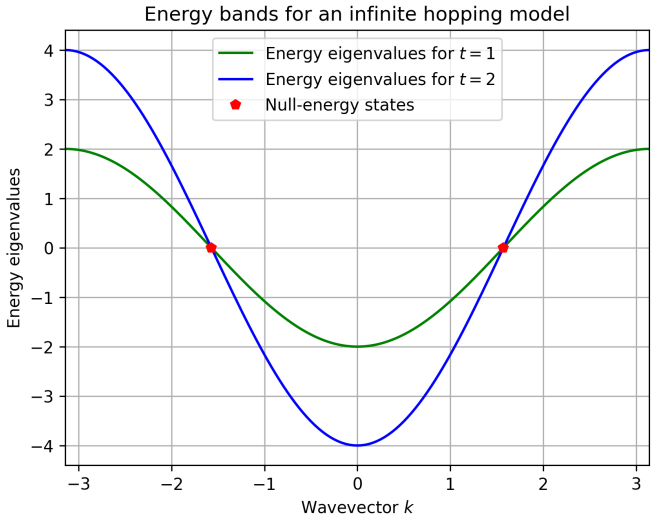

Fig. 2.5: Energy spectrum for an infinite chain.

picked a subsystem $\mathcal{A}$ as sketched in Fig.(2.4) and starting from Eq.(2.1.8), it is just a matter of studying the limit for N going to infinite of:

$$C_{mn} = \frac{1}{N}\frac{\sin\left[k(\bar{q})(m-n)+\frac{\pi}{N}(m-n)\right]}{\sin\left[\frac{\pi}{N}(m-n)\right]} \xrightarrow[N\to\infty]{} \frac{1}{\pi(m-n)}\sin\left[\frac{\pi}{2}(m-n)\right]. \qquad (2.1.11)$$

and let the code run for all pair of indexes $m, n \in \mathcal{A}$. In Fig.(2.6) the evolution of Von Neumann entropy is plotted for a subsystem of size M ranging from 1 to 300 sites. As anticipated, this time $S_{\mathcal{A}}$ has a different behaviour and shows a logarithmic growth. Fitting numerical results with CFT predictions, Eq.(1.3.21), we recover the same values for the central charge $c = 1$ and the constant $c_1' = 0.73$, proving once more the reliability of the code.

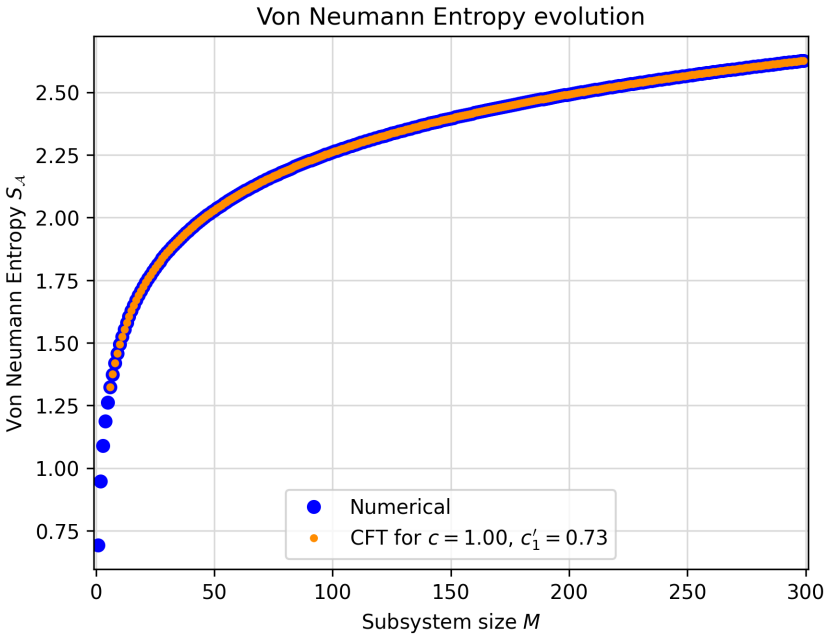

Fig. 2.6: Von Neumann entropy evolution for subsystem size M varying from 1 to 300.

2.2 SSH model

The follow-up in the analysis of free fermionic chains is the 1-dimensional *SSH model*[32], once more assuming in the first place finite dimension and periodic boundary condition. A very detailed analysis is provided in this case as this is the model I will focus on for the remaining part of the elaborate. SSH describes a so called dimerized chain consisting in an hopping model with alternating

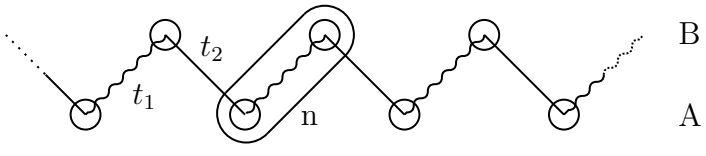

Fig. 2.7: SSH model.

parameters $t_1 \neq t_2$. The limit case for $t_1 = t_2$ just relates to the previous sections.

2.2.1 Finite dimensional chain

Starting from the finite dimensional case, SSH chains are described by hamiltonians of the form:

$$\hat{H} = \sum_{n=0}^{N-1} \Big[t_1 \Big(|2n\rangle \langle 2n+1| \Big) + t_2 \Big(|2n+1\rangle \langle 2n+2| \Big) + h.c. \Big], \tag{2.2.1}$$

or, in second quantization formalism:

$$\hat{H} = \sum_{n=0}^{N-1} \Big[t_1 \Big(c_{2n}^{\dagger} c_{2n+1} + c_{2n+1}^{\dagger} c_{2n} \Big) + t_2 \Big(c_{2n+1}^{\dagger} c_{2n+2} + c_{2n+2}^{\dagger} c_{2n+1} \Big) \Big]. \tag{2.2.2}$$

There exists even a third formulation involving the notion of sub-lattices. Sub-lattices can be observed in Fig.(2.7) and using them the hamiltonian becomes:

$$\hat{H} = \sum_{n=0}^{N-1} \Big[t_1 \Big(|n, A\rangle \langle n, B| \Big) + t_2 \Big(|n, B\rangle \langle n+1, A| \Big) + h.c. \Big] \tag{2.2.3}$$

. Note that, independently from the formulation chosen, n is no longer a site index as before but it turned in a cell index essentially. The process to diagonalize the hamiltonian this time is more articulated but still crucial to be able to determine the groundstate in a similar fashion as before. In the following lines I summarized it by providing the main results.

Acknowledging SSH also enjoys a translational symmetry, this time brought in by a slightly different operator:

$$\hat{T} = \sum_{n=0}^{N-1} \Big(|n+1, A\rangle \langle n, A| + |n+1, B\rangle \langle n, B| \Big), \tag{2.2.4}$$

we are prone to move again to momentum space. In this case, however, it is necessary to introduce 2 sets of plane waves, one localized on sub-lattice A and one on B:

$$|\tilde{k}(q)_+\rangle = \frac{1}{\sqrt{N}} \sum_{n=0}^{N-1} e^{ik(q)n} |n, A\rangle , \tag{2.2.5}$$

$$|\tilde{k}(q)_-\rangle = \frac{1}{\sqrt{N}} \sum_{n=0}^{N-1} e^{ik(q)n} |n, B\rangle . \tag{2.2.6}$$

Recasting $\hat{H}$ in terms of Eqs.(2.2.5),(2.2.6) results in matrix blocks $\hat{\tilde{H}}_q \in \mathcal{M}_{2x2}$ of the form:

$$\hat{\tilde{H}}_q = \begin{pmatrix} 0 & t_1 + t_2\, e^{-ik(q)} \\ t_1 + t_2\, e^{ik(q)} & 0 \end{pmatrix} \quad for\ q = 0, \cdots, N-1. \tag{2.2.7}$$

Evidently additional manipulations are required to fully diagonalize the problem but, from

matrices (2.2.7), it is already possible to derive the relation for eigenvalues and outline the energy spectrum. Readily one has:

$$E_q = \pm\sqrt{t_1^2 + t_2^2 + 2t_1 t_2 \cos[k(q)]}, \tag{2.2.8}$$

and, expressing staggered parameters as:

$$\begin{aligned} t_1 &= t(1+\delta), \\ t_2 &= t(1-\delta), \end{aligned} \tag{2.2.9}$$

allows us to plot the energy bands for different δ as in Fig.(2.8(a)). Looking at them, it straightforward to realize how the introduction of a parameter $\delta \neq 0$ causes the presence of a gap between the two bands of width 4δ. Systems with a similar energy spectrum are in fact known as gapped system and are generally used to model insulators.

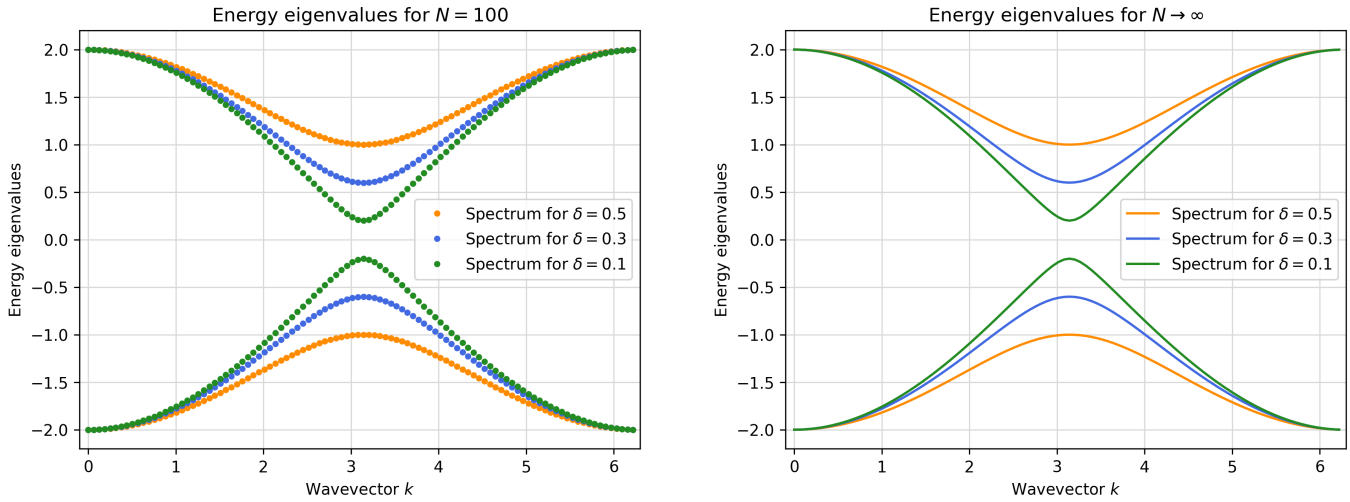

(a) Energy spectrum for $N = 100$.

(b) Energy spectrum limit for an infinite chain.

Fig. 2.8: SSH model's energy spectra evolution towards the limit for N going to infinite for $t = 1$ for $\delta = 0.5, 0.3, 0.1$.

The definition of a brand new set of operators is then required to fulfill diagonalization, let us therefore introduce $\{\alpha_q, \beta_q\}_{q=1,\cdots,N-1}$. Such operators must satisfy the usual canonical anti-commutation relations in order to preserve the fermionic nature of the underlying theory and are obtained from the transformations:

$$\begin{pmatrix} \tilde{c}_{q+} \\ \tilde{c}_{q-} \end{pmatrix} = U_q \begin{pmatrix} \alpha_q \\ \beta_q \end{pmatrix} \quad \xleftrightarrow[\text{complex conjugation}]{} \quad \begin{pmatrix} \tilde{c}^\dagger_{q+} \\ \tilde{c}^\dagger_{q-} \end{pmatrix} = U_q^* \begin{pmatrix} \alpha_q^\dagger \\ \beta_q^\dagger \end{pmatrix}, \tag{2.2.10}$$

with U_q being the unitary matrix that diagonalizes $\hat{\tilde{H}}_q$:

$$U_q = \begin{pmatrix} \frac{1}{\sqrt{2}} & -\sqrt{\frac{\eta_{q_-}}{2\eta_{q_+}}} \\ \sqrt{\frac{\eta_{q_+}}{2\eta_{q_-}}} & \frac{1}{\sqrt{2}} \end{pmatrix} \quad \textit{for: } \eta_{q_+} = t_1 + t_2\, e^{ik(q)} = \eta^*_{q_-}. \tag{2.2.11}$$

According to this formulation, it can be proven $\alpha^\dagger_q/\alpha_q$ are the operators related to positive energy states while $\beta^\dagger_q/\beta_q$ to negative ones. The definition of the groundstate, intended again as the zero temperature filled Fermi's sea, thus follows as:

$$|gs\rangle = \prod_{q=0}^{N-1} \beta^\dagger_q \,|0\rangle\,, \tag{2.2.12}$$

and will serve once more as the reference state to construct the correlation matrix C.

Recalling n plays the role of cell index for the SSH model, each element C_{mn} actually counts 4 different terms as it keeps in account all possible interactions between the particles of the m^{-th}, n^{-th} cells. Intuitively, this can be sketched in a clear way using matrix representation:

$$C_{mn} = \langle gs|c^\dagger_m c_n|gs\rangle = \begin{pmatrix} \langle c^\dagger_{m,A}\, c_{n,A}\rangle & \langle c^\dagger_{m,A}\, c_{n,B}\rangle \\ \langle c^\dagger_{m,B}\, c_{n,A}\rangle & \langle c^\dagger_{m,B}\, c_{n,B}\rangle \end{pmatrix}. \tag{2.2.13}$$

Finding their direct expressions for every A-B combination is thus our next goal. For a matter of clarity, let me first disclose explicitly the decomposition rules for momentum operators:

$$\begin{cases} \tilde{c}^\dagger_{q_+} = \frac{1}{\sqrt{2}}\left[\alpha^\dagger_q - \sqrt{\frac{\eta_{q_+}}{\eta_{q_-}}}\beta^\dagger_q\right] \\ \tilde{c}^\dagger_{q_-} = \frac{1}{\sqrt{2}}\left[\sqrt{\frac{\eta_{q_-}}{\eta_{q_+}}}\alpha^\dagger_q + \beta^\dagger_q\right] \end{cases} \xleftrightarrow[c.c.]{} \begin{cases} \tilde{c}_{q_+} = \frac{1}{\sqrt{2}}\left[\alpha_q - \sqrt{\frac{\eta_{q_-}}{\eta_{q_+}}}\beta_q\right] \\ \tilde{c}_{q_-} = \frac{1}{\sqrt{2}}\left[\sqrt{\frac{\eta_{q_+}}{\eta_{q_-}}}\alpha_q + \beta_q\right] \end{cases} \tag{2.2.14}$$

as an helpful intermediate step to refer in the upcoming computations.

- A-A correlation term, $C_{mn,AA}$:

$$\begin{aligned} C_{mn,AA} = \langle c^\dagger_{m,A}\, c_{n,A}\rangle &= \left[\frac{1}{N}\sum_{q,p=0}^{N-1} e^{-i[k(q)m - k(p)n]}\right]\langle \tilde{c}^\dagger_{q_+}\tilde{c}_{p_+}\rangle = \\ &= \left[\frac{1}{N}\sum_{q,p=0}^{N-1} e^{-i[k(q)m-k(p)n]}\right]\left[\frac{1}{2}\right]\langle \beta^\dagger_q\beta_p\rangle = \left[\frac{1}{2N}\sum_{q,p=0}^{N-1} e^{-i[k(q)m-k(p)n]}\right]\delta_{q,p} = \\ &= \frac{1}{2N}\sum_{q=0}^{N-1} e^{-ik(q)[m-n]} = 0. \end{aligned} \tag{2.2.15}$$

Differently from the result obtained for the hopping model, in this case the series

sums over all possible values of $q = 0, \cdots, N-1$, ending in a trivial outcome.

- B-B correlation term $C_{mn,BB}$ behaves precisely as the previous one since its decomposition leads to the very same expression:

$$\begin{aligned} C_{mn,BB} = \langle c^\dagger_{m,B}\, c_{n,B}\rangle &= \left[\frac{1}{N}\sum_{q,p=0}^{N-1} e^{-i[k(q)m-k(p)n]}\right]\langle \tilde{c}^\dagger_{q_-}\,\tilde{c}_{p_-}\rangle = \\ &= \left[\frac{1}{N}\sum_{q,p=0}^{N-1} e^{-i[k(q)m-k(p)n]}\right]\left[\frac{1}{2}\right]\langle \beta^\dagger_q \beta_p\rangle = 0. \end{aligned} \tag{2.2.16}$$

- A-B correlation term $C_{mn,AB}$:

$$\begin{aligned} C_{mn,AB} = \langle c^\dagger_{m,A}\, c_{n,B}\rangle &= \left[\frac{1}{N}\sum_{q,p=0}^{N-1} e^{-i[k(q)m-k(p)n]}\right]\langle \tilde{c}^\dagger_{q_+}\,\tilde{c}_{p_-}\rangle = \\ &= \left[\frac{1}{N}\sum_{q,p=0}^{N-1} e^{-i[k(q)m-k(p)n]}\right]\left[-\frac{1}{2}\sqrt{\frac{\eta_{q_+}}{\eta_{q_-}}}\right]\langle \beta^\dagger_q \beta_p\rangle = \\ &= -\frac{1}{2N}\sum_{q=0}^{N-1} e^{-ik(q)[m-n]}\sqrt{\frac{t_1 + t_2\, e^{ik(q)}}{t_1 + t_2\, e^{-ik(q)}}}. \end{aligned} \tag{2.2.17}$$

  The opposite correlation term $C_{mn,BA}$ can be derived from Eq.(2.2.17) upon complex conjugation of the terms inside the square root. As a matter of fact $C_{mn,AB} = C_{nm,BA}$ must hold.

Before moving on with the analysis of entanglement entropy, let me point out how, computationally wise, the workload already increases a lot here: mixed terms from the correlation matrix can be in fact only esteemed summing every single contribute at time as no further simplification have been spotted. Looking at Figs.(2.9(a)),(2.9(b)) very different behaviours arise compared to hopping model. Clearly, both of them can be traced back to the introduction of the half-gap parameter δ.

Commencing from the so called *saturation phenomenon*, this is a consequence of the system not being at criticality. As soon as this happens, correlation functions lose their power law nature and start to decay exponentially with a finite correlation length ξ[1]. In such condition CFT's methods are no longer applicable. More details can be found in the introduction of [33]. Still, it can be observed how, before reaching a *plateau*, $S_\mathcal{A}$ follows very accurately the trend of the system at criticality within a certain interval. Such circumstance can be explained in relation to the dimension of the subsystem: if M is small enough with respect to the correlation length the exponential decay does not drop sufficiently fast inside the partition and the subsystem behaves like it is still at criticality. In Fig.(2.9(a)) this is the case for $\delta = 0.001$ for which $S_\mathcal{A}$ never splits from the critical

[1]Recalling the usual notation for correlation lengths, here ξ should not be confused with the eigenvanlues of $C_\mathcal{A}$.

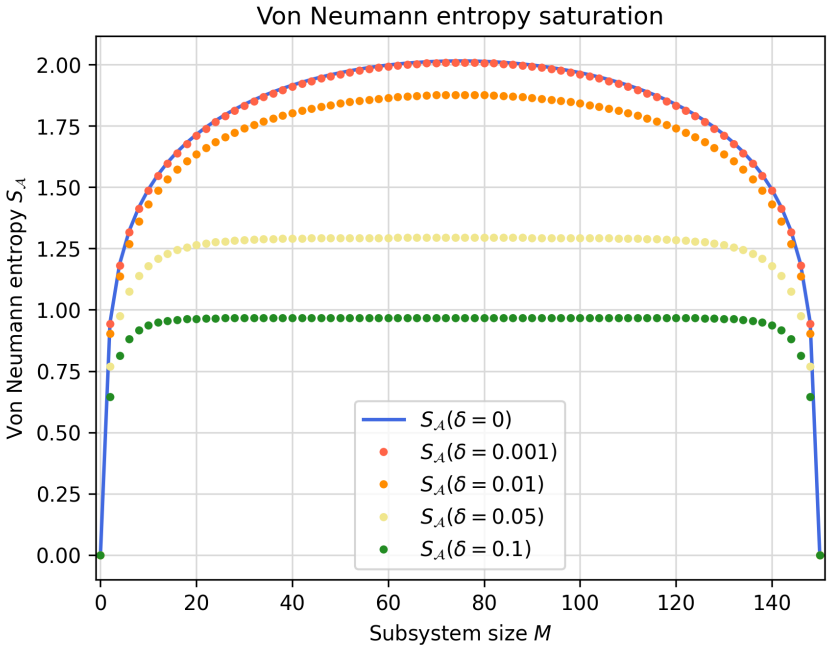

(a) $S_\mathcal{A}$ saturation phenomenon.

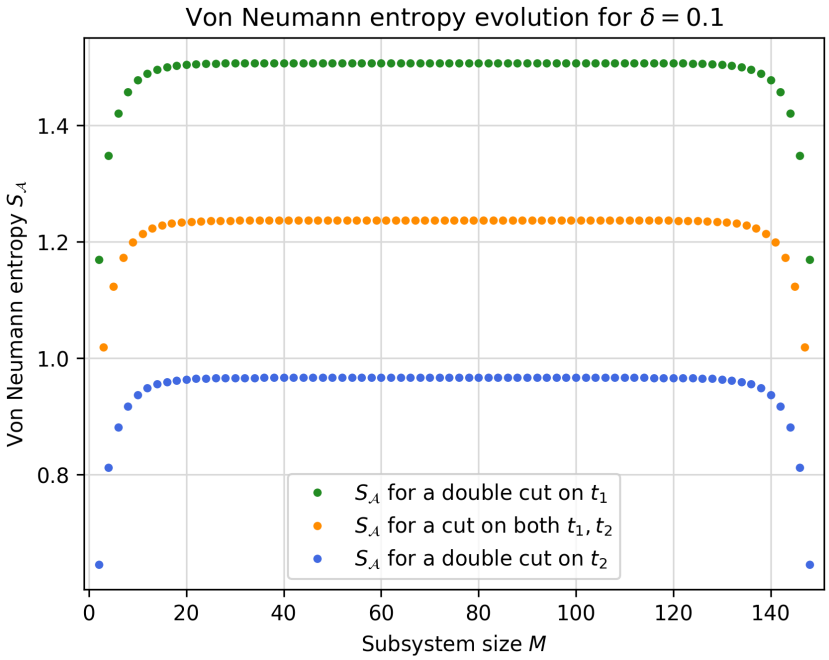

(b) $S_\mathcal{A}$ in different cut scenarios.

Fig. 2.9: Relevant traits of Von Neumann for a finite SSH model.

prediction. Analyzing the exponential decay in relation to δ, Fig.(2.10), it can be stated correlation length scales approximately as $\xi \propto \delta^{-1}$. No need to mention, the more δ is close to zero, the more Von Neumann entropy resembles Fig.(2.3(b)).

Pointing the attention at Fig.(2.9(b)) the strong dependence of Von Neumann entropy on subsystem boundaries emerges. It should not surprise, in fact, how performing a double

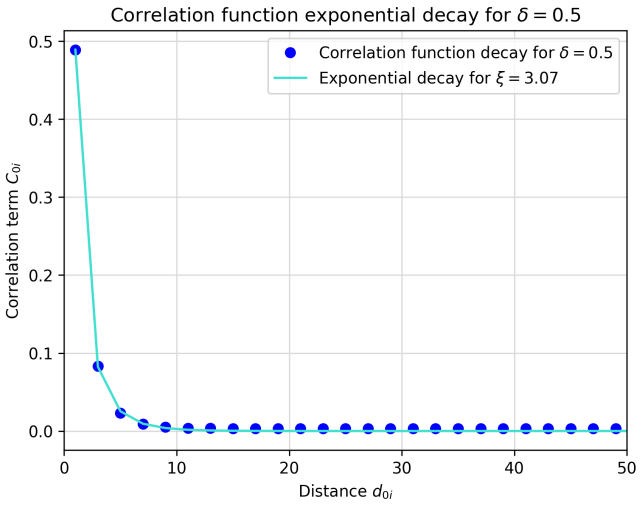

(a) Exponential decay for $\delta = 0.5$.

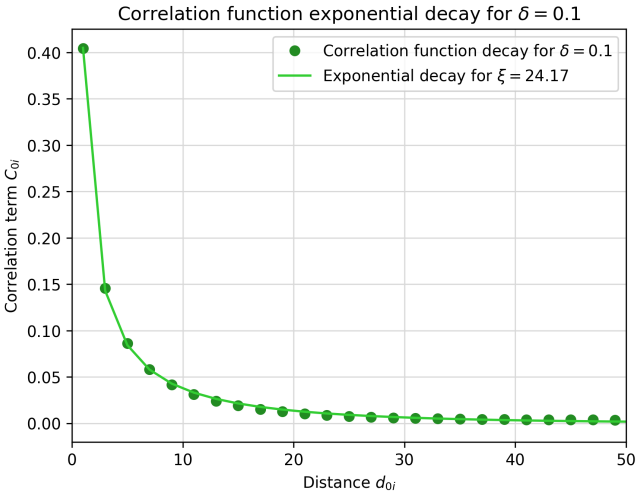

(b) Exponential decay for $\delta = 0.1$.

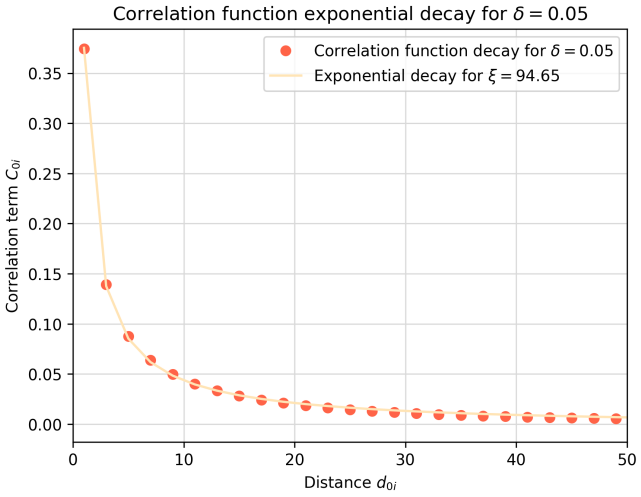

(c) Exponential decay for $\delta = 0.05$.

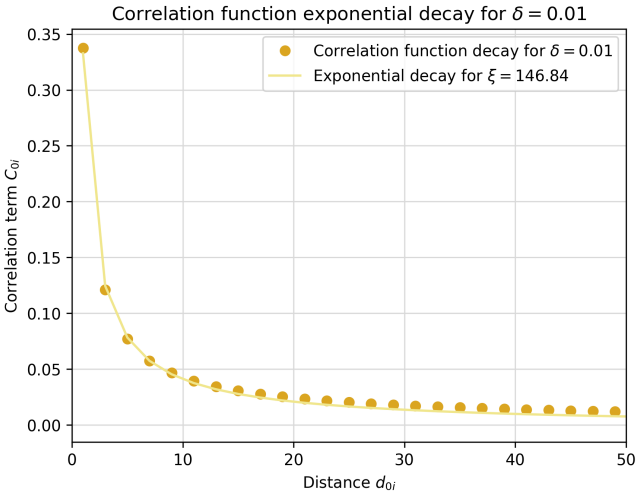

(d) Exponential decay for $\delta = 0.01$.

Fig. 2.10: Correlation lengths for $\delta = 0.5, 0.1, 0.05, 0.01$.

cut on two strong links t_1 (SS) instead of two weak ones t_2 (WW) results in completely different values of $S_{\mathcal{A}}$, regardless M being the same. Such fact should appear even more reasonable considering the limit for $\delta = 1$. In this case one usually says the chain is completely dimerized: weak links no longer exist thus performing a cut on t_2 would contribute with no entanglement at all.

2.2.2 Infinite dimensional chain

As for the hopping model, letting $N \to \infty$ allows us to move to the infinite chain scenario. While the energy spectrum can be derived rather straightforwardly and was already provided aside its discrete counterpart in Fig.(2.8(b)), adapting the formulae to derive the correlation matrix is quite challenging. First of all, starting from Eq.(2.2.17), one must

recast the series into an integral to be able to compute it. In particular, since the extremes of integration would go to infinite, for the sake of simplicity it is simpler to consider as variable of integration the wavevector k given its domain is finite. It thus follows:

$$\begin{aligned} C_{mn,AB} = -\frac{1}{2N}\sum_{q=0}^{N-1} e^{-ik(q)[m-n]}\sqrt{\frac{t_1+t_2\,e^{ik(q)}}{t_1+t_2\,e^{-ik(q)}}} \\ \xrightarrow[N\to\infty]{q\to k(q)} \quad -\int_{-\pi}^{\pi}\frac{dk}{4\pi}e^{-ik(m-n)}\sqrt{\frac{t_1+t_2e^{ik}}{t_1+t_2e^{-ik}}}. \end{aligned} \tag{2.2.18}$$

This formula would be already acceptable to build a code around it but very costly computationally. With few manipulations however, it is possible to achieve a very satisfactory result to reduce the execution time. To not interrupt abruptly the flow of the thesis, here I just provided the final result, relegating the whole procedure in appendix(A):

$$C_{mn,AB} \equiv \frac{1}{2}a_{n-m} = \frac{1}{2}a_r = \begin{cases} \frac{\epsilon^r}{2}\binom{-\frac{1}{2}}{r}\frac{\Delta_+}{\Gamma(\frac{1}{2})^2}\int_0^1 dt\ \frac{t^{r-\frac{1}{2}}(1-t)^{-\frac{1}{2}}}{(1-zt)^{-\frac{1}{2}}} & \textit{if: } r>0, \\ \frac{\epsilon^{-r}}{2}\binom{\frac{1}{2}}{-r}\frac{\Delta}{\Gamma(-\frac{1}{2})\Gamma(\frac{3}{2})}\int_0^1 dt\ \frac{t^{-r-\frac{3}{2}}(1-t)^{\frac{1}{2}}}{(1-zt)^{\frac{1}{2}}} & \textit{if: } r<0. \end{cases} \tag{2.2.19}$$

Using the above result it is possible to completely determine $C_{\mathcal{A}}$ and thus derive its eigenvalues.

At this point, following the *modus operandi* for the finite SSH chain, Von Neumann Entropy is analyzed with an eye on saturation and different cut possibilities. In Fig.(2.11) the evolution of $S_{\mathcal{A}}$ for different subsystem sizes M and various δ is plotted. For an infinite chain the subsystem has no theoretical limitation concerning its size M: this allows to simulate also very big subsystems and thus appreciate the effect of saturation even for considerably small values of δ as $\delta = 10^{-3}$ or $\delta = 10^{-4}$. Starting from the left picture, Fig.(2.11(a)), saturation is only visible for δ down to 10^{-2} as M ranges just from $[0, 160]$. However, extending its range to $M \in [0, 1000]$, Fig.(2.11(b)) on the right, compels also the gap for $\delta = 10^{-3}$ to become significant while $S_{\mathcal{A}}(10^{-4})$ slightly separates from critical behaviour only at the very end . All in all, saturation is again expected when $M \propto \delta^{-1}$.

Regarding different cut scenarios, no further comments are needed since the outcomes are essentially identical to the one observed for a finite chain. In this regard, plots in Fig.(2.9(b)) and Fig.(2.12) are very relatable with Von Neumann entropy splitting in 3 different branches.

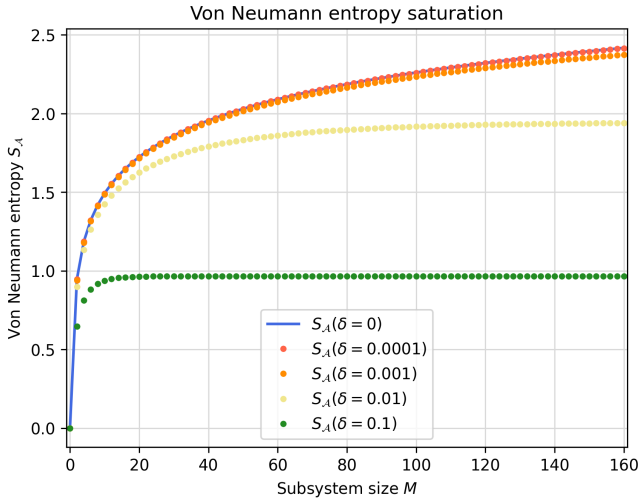

(a) $S_\mathcal{A}$ saturation phenomenon for $M \in [0, 160]$.

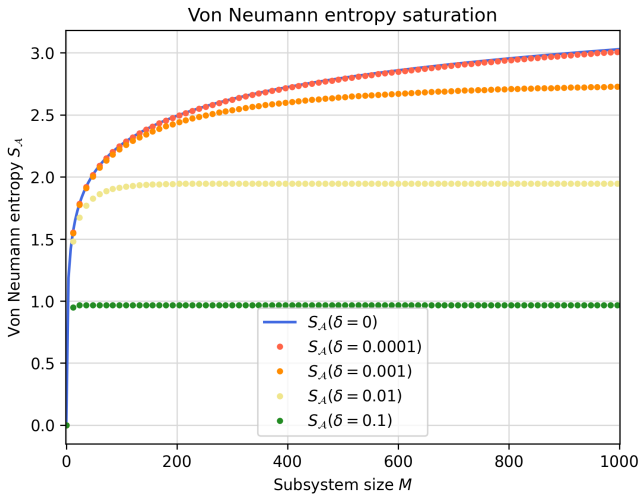

(b) $S_\mathcal{A}$ saturation phenomenon for $M \in [0, 1000]$.

Fig. 2.11: Von Neumann entropy saturation for a finite subsystem in an infinite SSH chain for different values of δ.

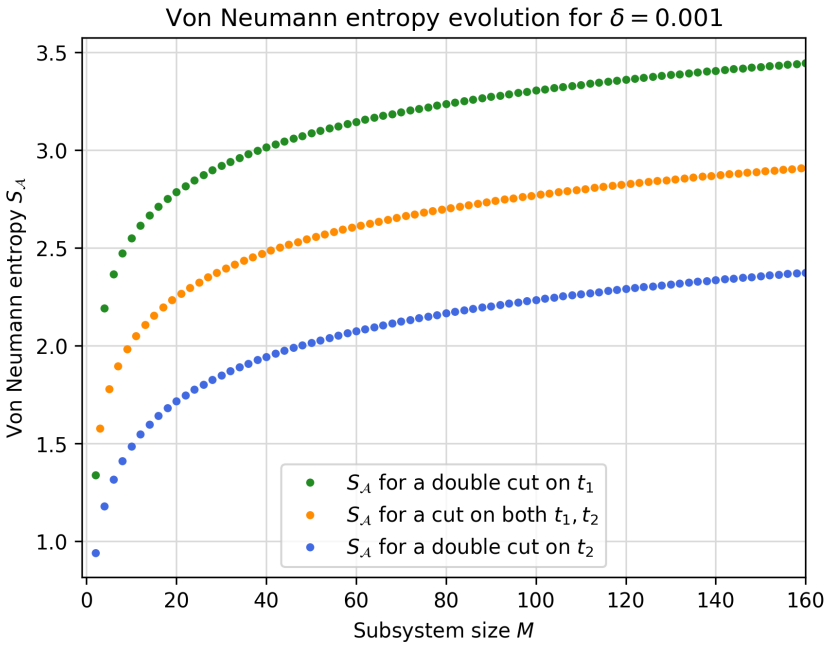

Fig. 2.12: $S_\mathcal{A}$ in different cut scenarios.

Chapter 3

Symmetry resolved entanglement entropies

Symmetries always played a crucial role in understanding physics and sorting out its complexity. One cannot help but acknowledging their importance as they are studied in a vast majority of fields, varying from classical to quantum domains, including entanglement measures. In this latter case, taking advantage of symmetries, allows us to better characterize entanglement.

To understand how, consider the example of a quantum many body system with an internal symmetry $U(1)$. Let ρ be its density matrix and $\hat{Q}$ the operator for the conserved quantity, it follows $[\rho, \hat{Q}] = 0$. Identified a bipartition of the total system $\mathcal{A}$-$\mathcal{B}$ and assuming the charge operator splits as $\hat{Q} = \hat{Q}_{\mathcal{A}} + \hat{Q}_{\mathcal{B}}$, relation $[\rho, \hat{Q}] = 0$ can be traced out over $\mathcal{B}$ finding $[\rho_{\mathcal{A}}, \hat{Q}_{\mathcal{A}}] = 0$. This implies $\rho_{\mathcal{A}}$ also admits a block-diagonal form as a direct consequence of the above premises. In particular, with respect to the eigenbase of $\hat{Q}_{\mathcal{A}}$, it can be expressed as:

$$\rho_{\mathcal{A}} = \oplus_q \hat{\Pi}_q \rho_{\mathcal{A}} = \oplus_q [p(q)\rho_{\mathcal{A}}(q)], \tag{3.0.1}$$

with $\hat{\Pi}_q$ being the projector on the charge sector related to the eigenvalue q, $\rho_{\mathcal{A}}(q)$ the corresponding collapsed version of the RDM and $p(q)$ the charge distribution in $\mathcal{A}$. Formally $p(q) \equiv \mathrm{Tr}(\Pi_q \rho_{\mathcal{A}})$ and is known as *full counting statistics* FCS in the literature[34][35]. Rephrasing $\rho_{\mathcal{A}}$ in charge sectors allows us to readily refine Von Neumann entropy:

$$\begin{aligned} S_{\mathcal{A}} &= -\,\mathrm{Tr}[\rho_{\mathcal{A}} \ln \rho_{\mathcal{A}}] = -\sum_q \langle \phi_q | \rho_{\mathcal{A}} \ln \rho_{\mathcal{A}} | \phi_q \rangle = \\ &= -\sum_q p(q) \ln p(q) - \sum_q p(q) S_{\mathcal{A}}(q) = \\ &\equiv S^f + S^c, \end{aligned} \tag{3.0.2}$$

where the definition of *symmetry resolved entanglement entropy* SREE has been introduced for:

$$S_{\mathcal{A}}(q) = \mathrm{Tr}[\rho_{\mathcal{A}}(q) \ln \rho_{\mathcal{A}}(q)]. \tag{3.0.3}$$

In Eq.(3.0.2) the first contribution, S^f, is the *Shannon entropy* linked to charge fluctuations while the second, S^c, is called *configurational entanglement entropy*[36] and measures

the total entropy due to each sector, each respectively weighted by $p(q)$.

In parallel, the definition extends to *symmetry resolved Rényi entropies* SRRE according to:

$$S_{n,\mathcal{A}}(q) = \frac{1}{1-n} \ln \mathrm{Tr}[\rho_{\mathcal{A}}^n(q)], \qquad \textit{for } n > 1. \tag{3.0.4}$$

EE are expected to spread evenly between charge sectors when $q - \langle \hat{Q}_{\mathcal{A}} \rangle$ is much smaller then the standard deviation of $\hat{Q}_{\mathcal{A}}$ itself. Such result is known as *entanglement equipartition* and has been proved for multiple systems.

The aim of this final chapter is that of studying SRRE for the SSH model, providing results able to match simulations' outcomes. Still, before proceeding, an additional piece of theory is necessary as evaluating symmetry resolved quantities using the equations above generally requires severe efforts. In the present case, starting from Eq.(3.0.4), SREE can be rephrased as:

$$S_{n,\mathcal{A}}(q) = \frac{1}{1-n} \ln \mathrm{Tr}\left[\left(\frac{\hat{\Pi}_q \rho_{\mathcal{A}}}{p(q)}\right)^n\right] = \frac{1}{1-n} \ln \frac{\mathrm{Tr}[(\hat{\Pi}_q \rho_{\mathcal{A}})^n]}{p(q)^n} = \frac{1}{1-n} \ln \left[\frac{Z_n(q)}{Z_1(q)^n}\right], \tag{3.0.5}$$

with the quantities $Z_n(q)$ corresponding to:

$$Z_n(q) \equiv \mathrm{Tr}[(\hat{\Pi}_q \rho_{\mathcal{A}})^n]. \tag{3.0.6}$$

Note $p(q)$ coincides exactly with $Z_1(q)$ and can be evaluated through its characteristic function:

$$\mathcal{Z}_1(\alpha) = \langle e^{i\alpha \hat{Q}_{\mathcal{A}}} \rangle = \mathrm{Tr}(e^{i\alpha \hat{Q}_{\mathcal{A}}} \rho_{\mathcal{A}}), \tag{3.0.7}$$

via Fourier transform:

$$Z_1(q) = \int_{-\pi}^{+\pi} \frac{d\alpha}{2\pi} e^{-i\alpha q} \mathcal{Z}_1(\alpha). \tag{3.0.8}$$

Generalizing the notion of characteristic function to any order n:

$$\mathcal{Z}_n(\alpha) = \mathrm{Tr}(e^{i\alpha \hat{Q}_{\mathcal{A}}} \rho_{\mathcal{A}}^n) \tag{3.0.9}$$

it is possible to determine all $Z_n(q)$ and thus fruitfully address the computation of SRRE without the need to extract the projectors Π_q. Objects in Eq.(3.0.9) are called *charged momenta* and will have therefore a central role in the upcoming sections.

3.1 SRRE in a finite subsystem in SSH

Charge operator $\hat{Q}$ in a free fermion chain generally corresponds to the number operator since the total number of particle is conserved. This means:

$$\hat{Q} = \sum_{j=0}^{N-1} \hat{n}_j \quad \xrightarrow[\text{restricting to } \mathcal{A}:]{} \quad \hat{Q}_{\mathcal{A}} = \sum_{j\in\mathcal{A}} \hat{n}_j, \tag{3.1.1}$$

but, for convenience, we will use:

$$\tilde{Q}_{\mathcal{A}} = \hat{Q}_{\mathcal{A}} - \langle \hat{Q}_{\mathcal{A}} \rangle = \sum_{j\in\mathcal{A}} (\hat{n}_j - \frac{1}{2}), \tag{3.1.2}$$

as it allows to considerably facilitate future expressions. Yet, some caution is needed as these advantages do not come completely for free: when M is odd, translating $\hat{Q}$ according to Eq.(3.1.2) implies it will turn into an half-integer. Replacing $\tilde{Q}_{\mathcal{A}}$ in the equation for charged momenta, Eq.(3.0.9), along with the corresponding RDM, one derives:

$$\begin{aligned} \mathcal{Z}_n(\alpha) &= \mathrm{Tr}\left[\otimes_{j\in\mathcal{A}} \Big((1-\xi_j)^n |0\rangle\langle 0|_j + \xi_j^n |1\rangle\langle 1|_j \Big) e^{i\alpha\tilde{Q}_{\mathcal{A}}} \right] = \\ &= \prod_{j\in\mathcal{A}} \Big[(1-\xi_j)^n e^{-i\frac{\alpha}{2}} + \xi_j^n e^{i\frac{\alpha}{2}} \Big]. \end{aligned} \tag{3.1.3}$$

Setting $\mathcal{A} = [1, M]$ and recalling the identity for the eigenvalues of $C_{\mathcal{A}}$ in Eq.(1.2.14), the above equation becomes:

$$\mathcal{Z}_n(\alpha) = \prod_{j=1}^{M/2} \Big[(1-\xi_j)^{2n} + \xi_j^{2n} + 2(1-\xi_j)^n (\xi_j)^n \cos(\alpha) \Big] \times \theta(M\%2) \Big[\Big(\frac{1}{2^n} \Big) 2\cos\Big(\frac{\alpha}{2} \Big) \Big], \tag{3.1.4}$$

with the $\theta(M\%2)$-term being there only when the size of the sub-system is odd. Let me point out how, in this latter case, charged momenta become anti-periodic. Once charged momenta are known, the problem is basically solved. It is then interesting to look at the behaviour of charge distribution FCS and SRRE, at different orders, and especially to consider how those quantities vary with respect to sub-system size.

On general grounds $p(q)$ is a gaussian distribution centered in zero with variance strongly conditioned by both δ and M. When the subsystem is taken to be close to criticality, Fig.(3.1), variance is given by the relation:

$$\sigma^2 = \frac{1}{\pi^2} \ln \frac{M}{2} + const, \tag{3.1.5}$$

and reasonably no differences emerge if cuts are performed on two weak (WW), two strong (SS) or mixed links (WS). In the example provided for $\delta = 10^{-4}$, the value of the

constant has been esteemed performing the fit in Fig.(3.1(b)). Replacing $const = 0.314$ in Eq.(3.1.5) and considering $M = 400$ one immediately recovers the variance $\sigma^2 = 0.848$ of Fig.(3.1(a)). This latter plot also highlights how, for different cuts, we obtain the very same distribution as all data can be fitted by a single gaussian.

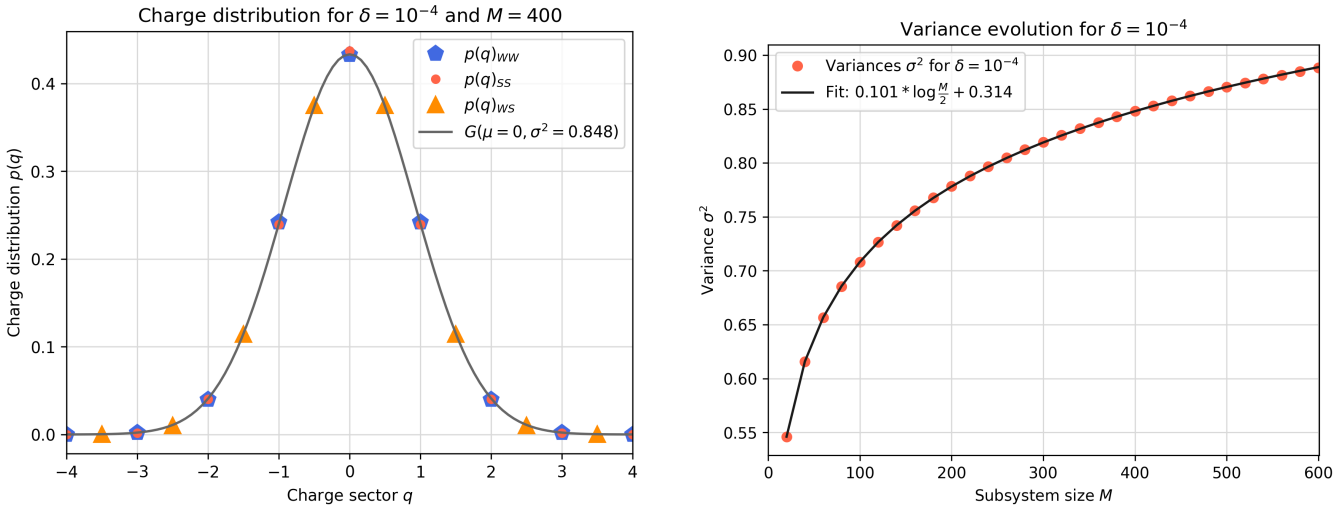

(a) Independence of $p(q)$ from cut edges.

(b) Logarithmic growth of variance σ^2.

Fig. 3.1: Behaviour of $p(q)$ and σ^2 in conditions resembling criticality. In **(a)** neutrality of $p(q)$ with respect to cutting conditions appear evident as all numerical data can be fitted by the same gaussian. In **(b)** the fit of Eq.(3.1.5) is plotted.

As the subsystem loses its critical-like behaviour, both $p(q)$ and σ^2 start feeling effects related to cuts. This can be observed in Fig.(3.2(a)) where distributions for WW, SS and WS no longer coincide and, for each of them, a different gaussian can be delineated. Concerning variance, Fig.(3.2(b)), again a phenomenon of saturation takes place.

Drawing the attention to symmetry resolved Rényi entropies $S_{n,\mathcal{A}}(q)$, depending on their order n, the corresponding charged momenta and Fourier transforms must be computed. In Fig.(3.3) a sketch of the various $Z_n(q)$ for n ranging from 1 to 5 is provided. As it can be observed, these functions behave in a similar way and tend to drop very quickly as soon as one moves from the origin. Also, the higher is the order n, the smaller is the distributions. When it comes to simulations, this turns out to be a strong limiting factor since the $Z_n(q)$, even for q just few units away from the origin, are already smaller than a float datatype precision, causing Eq.(3.0.5) to be unusable. To overcome such constraint the more natural solution would be to use a more precise datatype but this has considerable consequences on execution times. To prevent such circumstance the focus has been thus directed uniquely to Rényi entropies of second order since, as it will be shown, without changing datatype it is already possible to compute their values in enough charge sectors to derive appreciable results. Second order SRRE ($S_{2,\mathcal{A}}(q)$) will thus be the main quantity under investigation from now on.

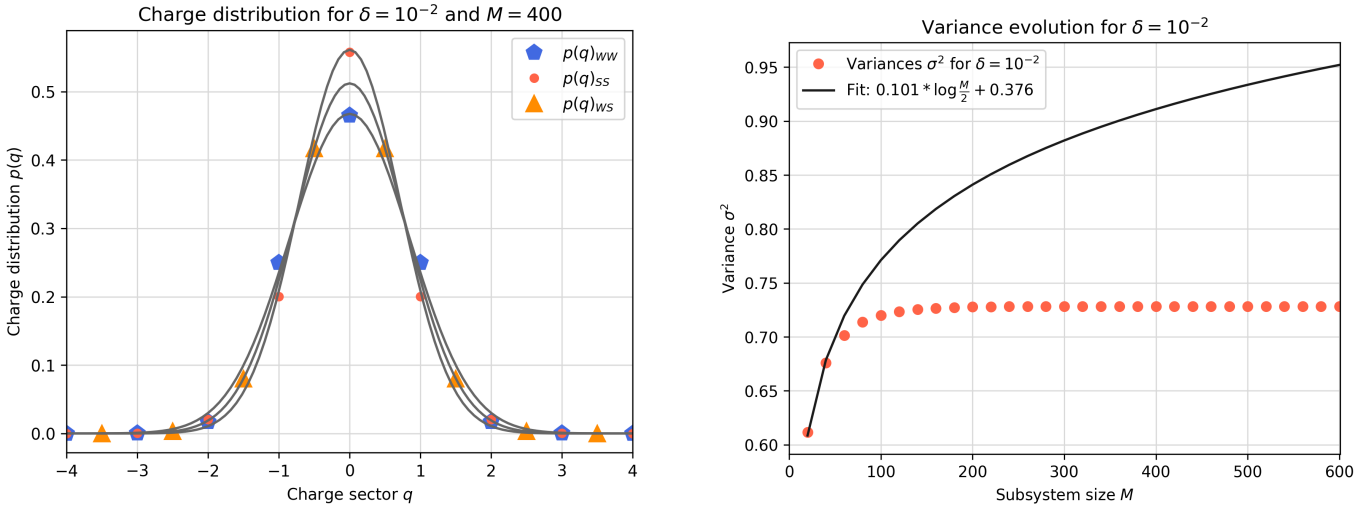

(a) Distinct charge distributions for WW, SS, WS.

(b) Saturation of σ^2.

Fig. 3.2: Behaviour of $p(q)$ and σ^2 in conditions far from criticality. in **(a)** charge distributions in the three scenarios, WW, SS, WS, are plotted. For each of them a different gaussian is derived as proof of their distinction. In **(b)** saturation phenomenon for variance is plotted.

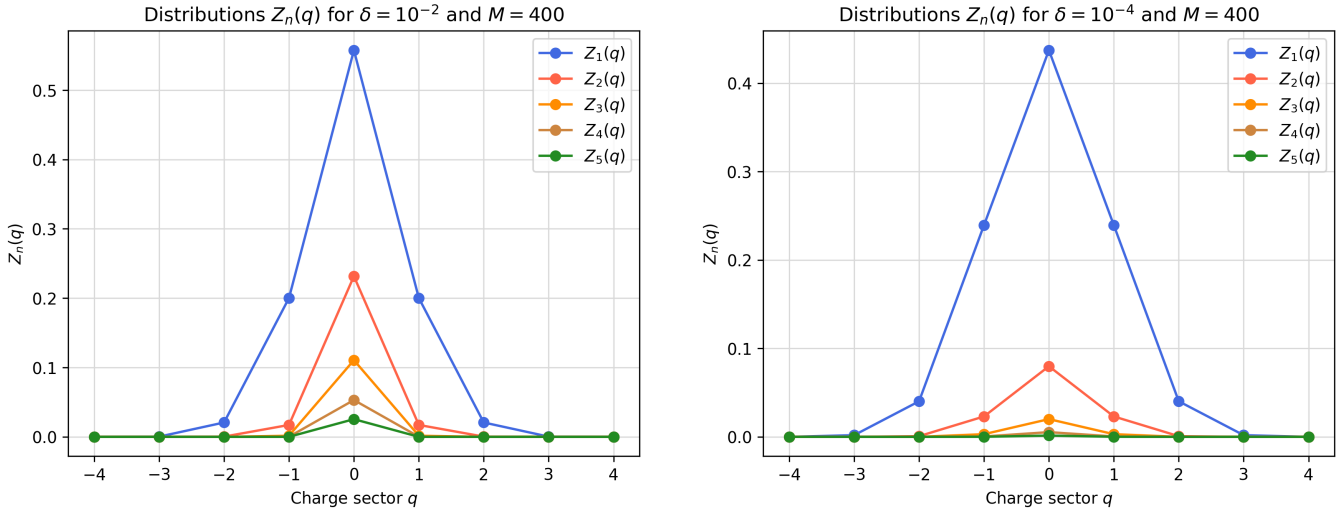

(a) Fourier transform for $\delta = 10^{-2}$.

(b) Fourier transform for $\delta = 10^{-4}$.

Fig. 3.3: Plots of Fourier transforms with the order n varying from 1 to 5 for: **(a)** $\delta = 10^{-2}$, **(b)** $\delta = 10^{-4}$.

By simulating and plotting $S_{2,\mathcal{A}}(q)$ varying parameters δ and M for all possible cutting scenarios WW, SS and WS; the presence of few recurrent patterns might be spotted. Fig.(3.4) and Fig.(3.5) are the some up of this process for which the most significant and understandable plots have been picked.

The first crucial aspect, recognizable even after a quick glance, is how the parity of M affects the behaviour of $S_{2,\mathcal{A}}(q)$. When M is odd, Fig.(3.4), Rényi entropies have a

regular behaviour while, when is odd, Fig.(3.5), they display an oscillating trend. Further, comparing WW and SS, another detail emerges: SRREs oscillate for both but with a complete opposite phase upon charge sector.

Finally, observing more carefully picture by picture, a recursive trait unfolds for M getting bigger as $S_{2,\mathcal{A}}(q)$ seems to converge to precise limits. Specifically, when M is even, Rényi entropy's oscillations sort of stabilize between two fixed extremes, viceversa, when M is odd, $S_{2,\mathcal{A}}(q)$ appears to flatten towards a constant value. This latter remark is what inspired us to consider subsystems of infinite dimension looking for a method to predict exactly SRRE in this limit.

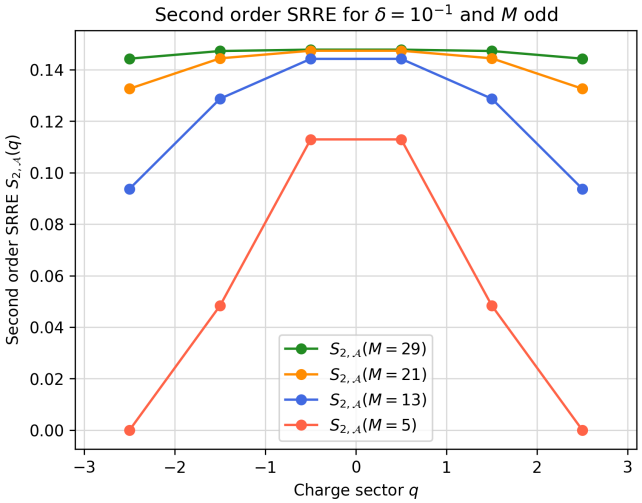

(a) WS cuts for $\delta = 0.1$.

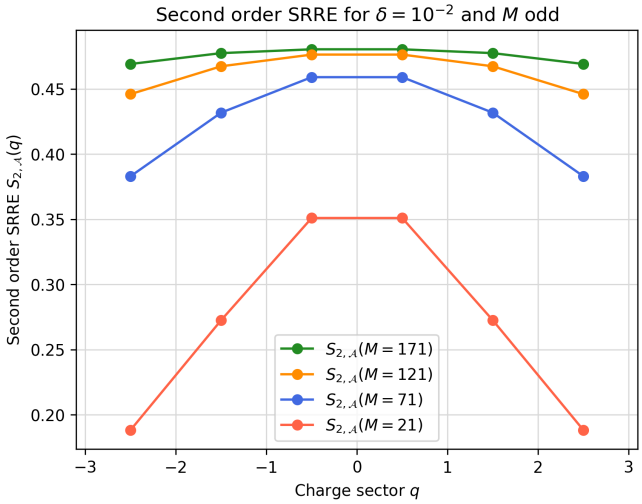

(b) WS cuts for $\delta = 0.01$.

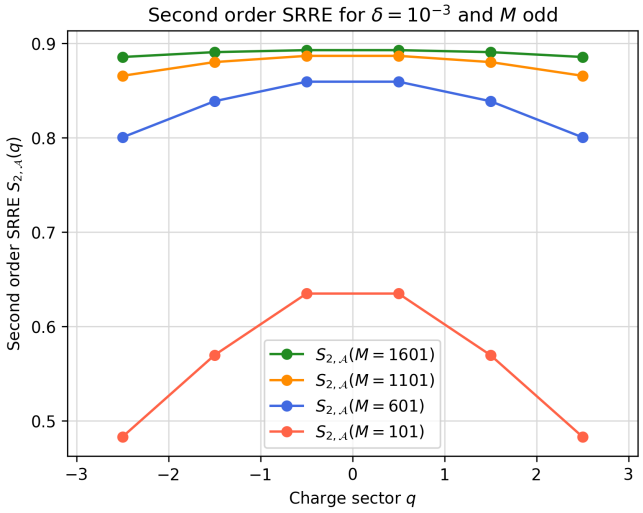

(c) WS cuts for $\delta = 0.001$.

Fig. 3.4: Second order SRRE behaviour for $\delta = 10^{-1}, 10^{-2}, 10^{-3}$ in cutting scenario WS.

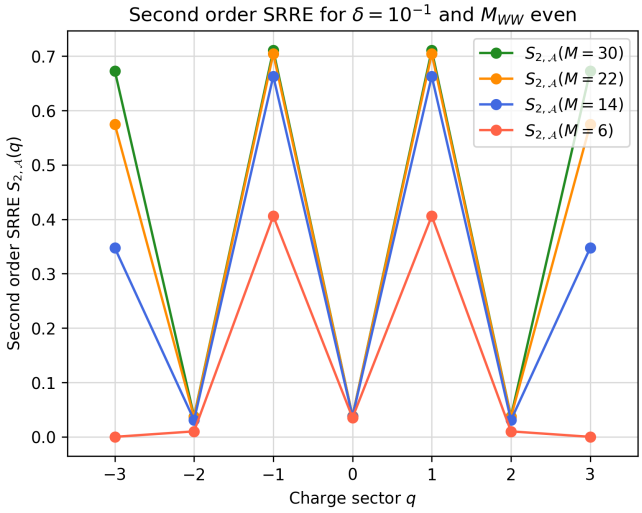

(a) WW cuts for $\delta = 0.1$.

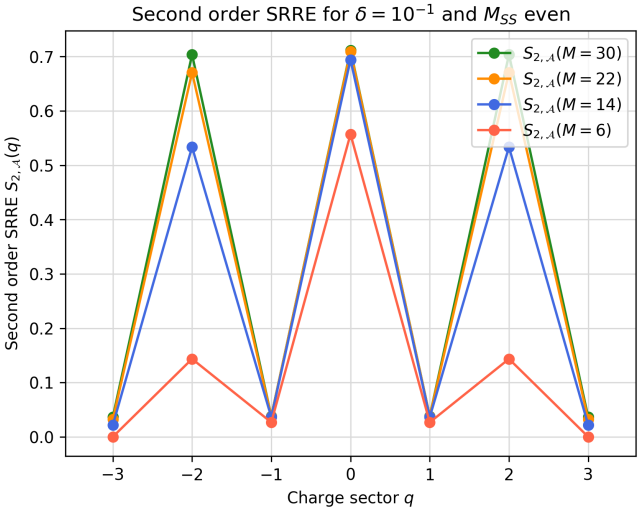

(b) SS cuts for $\delta = 0.01$.

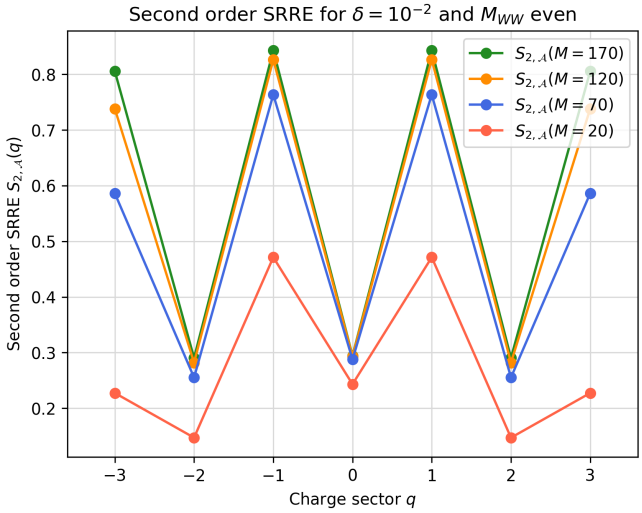

(c) WW cuts for $\delta = 0.01$.

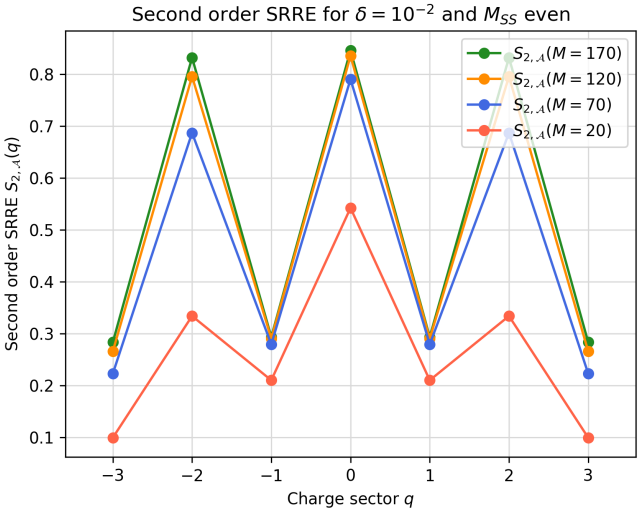

(d) SS cuts for $\delta = 0.01$.

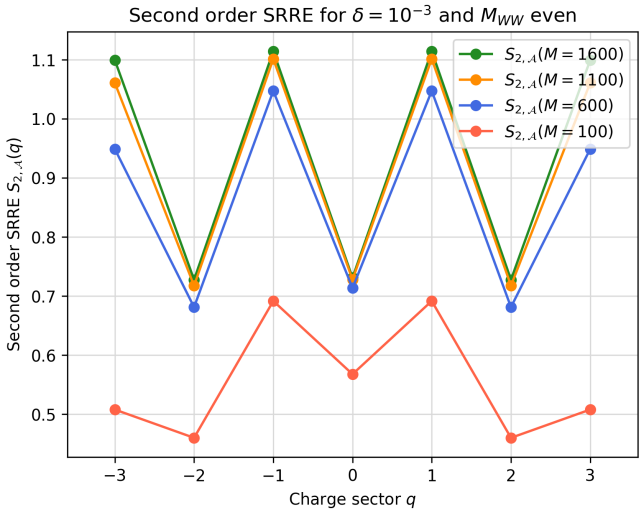

(e) WW cuts for $\delta = 0.001$.

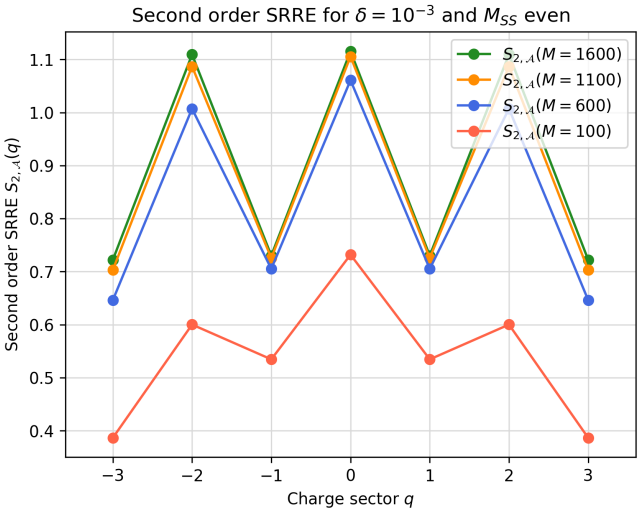

(f) SS cuts for $\delta = 0.001$.

Fig. 3.5: Second order SRRE behaviour for $\delta = 10^{-1}, 10^{-2}, 10^{-3}$ in cutting scenarios WW and SS.

3.2 SRRE in an infinite subsystem in SSH

Thinking about it, this problem shows up as an impossible one to solve, at least with the elements of theory discussed in previous chapters. To an infinite subsystem, in fact, it corresponds an infinite dimensional reduced correlation matrix $C_{\mathcal{A}} \in \mathcal{M}_{\infty\times\infty}$ for which solving the eigenvalue problem numerically is just an helpless task. Still, SSH model admits another procedure to determine its entanglement spectrum and, in particular, this is an analytical one[37]. Before outlining the machinery behind it, let me point out how, unlike for finite subsystem, this time even a single cut can be enough to isolate $\mathcal{A}$ as the other end of the chain just goes to infinite.

Introducing the quantities:

$$\chi = \exp\Big[-\pi\frac{I(k')}{I(k)}\Big] \qquad with: \quad I(k) = \int_0^1 \frac{dt}{\sqrt{(1-t^2)(1-k^2t^2)}} \tag{3.2.1}$$

and:

$$k = \begin{cases} \epsilon & if:\ \epsilon^2 < 1 \ \leftrightarrow\ \delta > 0 \\ \epsilon^{-1} & if:\ \epsilon^2 > 1 \ \leftrightarrow\ \delta < 0 \end{cases}, \qquad k' = \sqrt{1-k^2}, \tag{3.2.2}$$

eigenvalues ξ_m of $C_{\mathcal{A}}$ are then given by:

$$\xi_m = \frac{1}{1+\chi^m} \qquad with: \begin{cases} m\ \ odd & if:\ \delta > 0, \\ m\ \ even & if:\ \delta < 0. \end{cases} \tag{3.2.3}$$

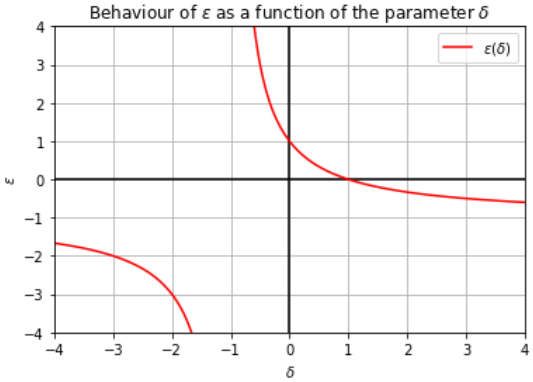

Fig. 3.6: Sketch of ϵ as a function of δ.

Note that no restrictions applies to m which can be also negative and in fact, eigenvalues ξ_m still satisfy the relation $\xi_m = 1 - \xi_{-m}$. In the interest of clarity, it should be pointed out Eq.(3.2.3) specifically generates eigenvalues for an half-infinite chain with a single cut on $(1-\delta)$ and not the other way around. Such distinction is supported by the following analysis of the limits $\delta \to \pm 1$:

- For $\delta < 0$, as a consequence of $m = 0$, one always has $\xi_0 = 0.5$. Taking the limit for $\delta \to -1$, this eigenvalue becomes the only non-trivial one as all others reduce to either 0's or 1's. Such eventuality is none but having a single cut taken in a dimer of a fully dimerized chain, id est, on its strong link S.

- On the other hand when $\delta > 0$, one has to use odd integers and shall consider

the opposite limit case. For $\delta \to 1$ one gets $\chi = 0$ and thus ends up with ξ_m being only 0's or 1's. Recalling Eq.(1.2.13), those are linked to a non-production of entanglement entropy for the subsystem which, in a dimerized chain, corresponds to performing a cut between two adjacent dimers, hence the weak link W of an SSH chain.

To eventually compose the full spectrum of an infinite subsystem with two edges it is enough to consider two sets of eigenvalues instead of one, paying attention to the types of cuts characterizing the partition. Taking as an example the case of subsystems with one boundary on a weak and one on a strong link (WS), one should combine the ξ_m's coming from the use of both even and odd integers. Similarly, if boundaries are two of the same type, one should just take a double copy of each ξ_m.

As a solidity check, we compared the entanglement spectra obtained analytically according to Eq.(3.2.3) with numerical results obtained using reduced correlation matrix method in a SSH chain far from criticality but with a finite size. In this latter case in fact, choosing a subsystem with M greater than δ^{-1} of few orders of magnitude, implies that the two boundaries barely communicate one with the other thus, up to exponentially small corrections, the subsystem is expected to behave as if it has infinite length. By virtue of completeness, an agreement up to the 13^{th} digit has been recorded for eigenvalues simulated with $M = 1000$ and $\delta = 0.05$.

Before moving on with the analysis of second order SRRE let me just make one last comment. Being analytical, this method would generate infinite many eigenvalues populating the spectrum. Nonetheless when it comes to coding only a bunch of them are really relevant as all the others are just close to either 0 or 1 beyond float precision. Speaking of this set of relevant eigenvalues, as δ becomes smaller and smaller, it counts more and more elements. This is a consequence of the variation of χ, Eq.(3.2.1), whose plot can be found in Fig.3.7(a). Accordingly, powers χ^m in Eq.(3.2.3) also increase causing the corresponding eigenvalues to detach from extreme values 0 or 1. Such *activation* of eigenvalues can be clearly observed in Fig.3.7(b),3.7(c) for few positive even indexes. All in all, the closer the system is to criticality, the wider the set of relevant eigenvalues get. Coherently with what we claimed before this is to be expected as to replicate this result via simulations we would need a bigger subsystem in order for the two edges not to communicate.

Using this analytical approach with explicit expressions for eigenvalues of the entanglement spectrum opens to the possibility of rephrasing Von Neumann entropy, Eq.(1.2.13).

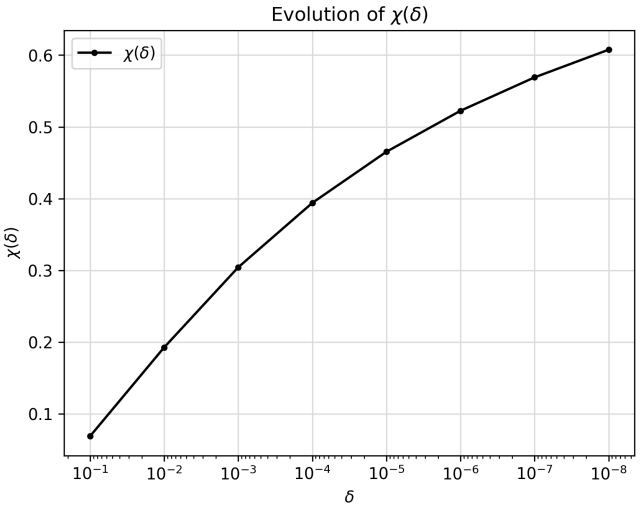

(a) Evolution of $\chi(\delta)$ plotted in reversed logarithmic scale for δ.

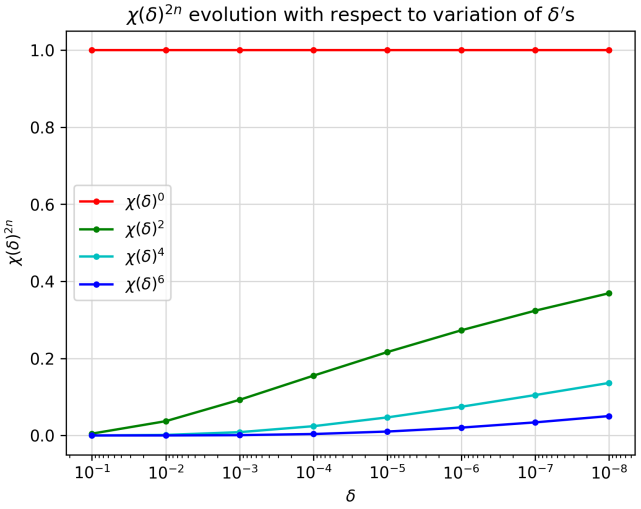

(b) Evolution of few $\chi^{2n}(\delta)$ powers plotted in reversed logarithmic scale for δ.

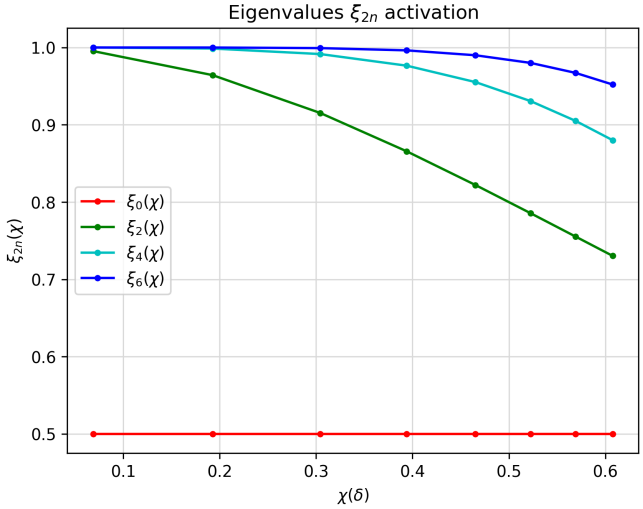

(c) Eigenvalues *activation* for $\chi(\delta)$ increasing.

Fig. 3.7: Plots of χ and eigenvalues activation ξ_{2m} for δ varying from 10^{-8} to 10^{-1}.

Depending on the edge scenario one starts with:

$$S = -\sum_{m\in\mathbb{Z}} \Big[\xi_m \ln \xi_m + (1-\xi_m)\ln(1-\xi_m)\Big] \;\; \textit{if WS}\,, \tag{3.2.4}$$

$$S = -2\sum_{m} \Big[\xi_m \ln \xi_m + (1-\xi_m)\ln(1-\xi_m)\Big] \;\; \textit{with:} \begin{cases} m \;\textit{odd, if WW,} \\ m \;\textit{even, if SS,} \end{cases} \tag{3.2.5}$$

with the presence of a prefactor 2 in WW-SS scenarios to remind ξ_m are two-fold degen-

erate when identical cuts are taken. From there, given the following identity:

$$\xi_m \ln \xi_m + (1-\xi_m)\ln(1-\xi_m) = \frac{\chi^m \ln(\chi^m)}{1+\chi^m} - \ln(1+\chi^m), \tag{3.2.6}$$

and recalling the relation for ξ_m and ξ_{-m}, we might reduce above formulae as:

$$S = \ln(2) - 2\ln(\chi)\Big[\sum_{m\in\mathbb{Z}^+}\Big(\frac{m\chi^m}{1+\chi^m}\Big)\Big] + 2\ln\Big[\prod_{m\in\mathbb{Z}^+}(1+\chi^m)\Big] \;\; \textit{if WS}\,, \tag{3.2.7}$$

$$S = \begin{cases} -4\ln(\chi)\Big[\sum_{m>0}\Big(\frac{m\chi^m}{1+\chi^m}\Big)\Big] + 4\ln\Big[\prod_{m>0}(1+\chi^m)\Big] & \textit{WW, m odd,} \\ 2\ln 2 - 4\ln(\chi)\Big[\sum_{m>0}\Big(\frac{m\chi^m}{1+\chi^m}\Big)\Big] + 4\ln\Big[\prod_{m>0}(1+\chi^m)\Big] & \textit{SS, m even,} \end{cases} \tag{3.2.8}$$

with $2\ln 2$ being the term due to $m = 0$ which has been taken out from sequences cause it has no counterpart ξ_{-0} or, to be the more precise, it is its own counterpart. Eq.(3.2.7),(3.2.8) have been tested comparing their results with numerical outcomes.

3.2.1 SRRE for an infinite half-chain

Addressed the problem of computing entanglement spectrum we can finally draw back the attention to second order SRRE. Recalling the equation for charge momenta, Eq.(3.1.4), the first task is to understand whether the dimension of our system is even or odd. However, since M is infinite, answering this question is a subtle point and we can only try to solve it using theoretical arguments.

Assuming the limit of a fully dimerized SSH we proved for an infinite half-chain with boundary on a strong link, that its entanglement spectrum becomes completely trivial except for $\xi_0 = \frac{1}{2}$. Being this the only relevant term we might conjecture that from the other end no contributions to entanglement entropy arise which implicitly implies the partition must end between two dimers, on a weak link. As a consequence, when the half-chain has the cut on S, M has to be treated as odd while, as soon as we include or remove an adjacent site, moving the cut on W, M turns even.

The analysis of the 2 cases follows. An additional index μ has been added to $\mathcal{Z}_n^{(\mu)}(\alpha)$ to distinguish them: $\mu = 0$ when the cut is on W, $\mu = 1$ vice versa. The former will be identified as *odd case* while the latter as *even case* due to the integers used to create their entanglement spectra.

The odd case (0)

Starting from Eq.(3.1.4) with M even and the summation running only over odd indexes, one gets:

$$\begin{aligned}
\mathcal{Z}_n^{(0)}(\alpha) &= \prod_{m\geq 1}\Big[(1-\xi_m)^{2n}+\xi_m^{2n}+(1-\xi_m)^n(\xi_m)^n 2\cos(\alpha)\Big] = \\
&= \prod_{m\geq 1}\Big[\Big(\frac{\chi^m}{1+\chi^m}\Big)^{2n}+\Big(\frac{1}{1+\chi^m}\Big)^{2n}+\Big(\frac{\chi^m}{(1+\chi^m)^2}\Big)^{n}2\cos(\alpha)\Big] = \\
&= \prod_{m\geq 1}\frac{[1+\chi^{2nm}+\chi^{nm}2\cos(\alpha)]}{(1+\chi^m)^{2n}} = \\
&= \prod_{l=1}^{\infty}\frac{(1+\chi^{n(2l-1)}e^{i\alpha})(1+\chi^{n(2l-1)}e^{-i\alpha})}{(1+\chi^{(2l-1)})^{2n}} = \\
&= \prod_{l=1}^{\infty}\frac{(1+\gamma^{2l-1}e^{i\alpha})(1+\gamma^{2l-1}e^{-i\alpha})}{(1+\chi^{(2l-1)})^{2n}},
\end{aligned} \tag{3.2.9}$$

where $\gamma=\chi^n$ has been introduced to simplify the expression. Next, taking into account the definition of the Jacobi theta function θ_3[38, (20.5.9)] for $p=e^{i\pi z}$ and $s=e^{i\pi\tau}$:

$$\theta_3(\pi z|\tau)\equiv\theta_3(p\,|\,s)=\prod_{l=1}^{\infty}(1-s^{2l})(1+s^{2l-1}p^2)(1+s^{2l-1}p^{-2})=\sum_{m=-\infty}^{\infty}p^{2m}s^{m^2}, \tag{3.2.10}$$

one can reformulate Eq.(3.2.9) as:

$$\begin{aligned}
\mathcal{Z}_n^{(0)}(\alpha) &= \prod_{l=1}^{\infty}\frac{(1-\gamma^{2l})}{(1-\gamma^{2l})}\frac{(1+\gamma^{2l-1}e^{i\alpha})(1+\gamma^{2l-1}e^{-i\alpha})}{(1+\chi^{(2l-1)})^{2n}} = \\
&= \prod_{l=1}^{\infty}\frac{(1+\gamma^{2l-1})^2}{(1+\gamma^{2l-1})^2}\frac{\theta_3(\frac{\alpha}{2},\gamma)}{(1-\gamma^{2l})(1+\chi^{(2l-1)})^{2n}} = \\
&= \frac{\theta_3(\frac{\alpha}{2},\gamma)}{\theta_3(0,\gamma)}\prod_{l=1}^{\infty}\frac{(1+\gamma^{2l-1})^2}{(1+\chi^{(2l-1)})^{2n}} = \\
&= \frac{\theta_3(\frac{\alpha}{2},\gamma)}{\theta_3(0,\gamma)}\prod_{l=1}^{\infty}\left[\frac{(1+\chi^{(2l-1)n})}{(1+\chi^{(2l-1)})^{n}}\right]^2 = \theta_3\Big(\frac{\alpha}{2},\gamma\Big)A_n^{(0)}.
\end{aligned} \tag{3.2.11}$$

At this stage, after Fourier transform, one derives:

$$Z_n^{(0)}(q)=A_n^{(0)}\gamma^{q^2}=A_n^{(0)}\chi^{nq^2}, \tag{3.2.12}$$

and in particular:

$$Z_1^{(0)}(q)=A_1^{(0)}\chi^{q^2}=\frac{1}{\theta_3(0,\chi)}\chi^{q^2}, \tag{3.2.13}$$

which has indeed the form of a gaussian distribution. Using Eq.(3.2.12) symmetry-resolved Rényi entropies reduce to:

$$\begin{aligned} S_n^{(0)}(q) &= \frac{1}{1-n}\ln\left[\frac{A_n^{(0)}}{(A_1^{(0)})^n}\right] = \frac{1}{1-n}\ln\left[\frac{\theta_3(0,\chi)^n}{\theta_3(0,\gamma)}\prod_{l=1}^{\infty}\left(\frac{(1+\chi^{(2l-1)n})}{(1+\chi^{(2l-1)})^n}\right)^2\right] = \\ &= \frac{1}{1-n}\ln\left[\prod_{l=1}^{\infty}\frac{(1-\chi^{2l})^n(1+\chi^{2l-1})^{2n}}{(1-\gamma^{2l})(1+\gamma^{2l-1})^2}\frac{(1+\gamma^{(2l-1)})^2}{(1+\chi^{(2l-1)})^{2n}}\right] = \\ &= \frac{1}{1-n}\ln\left[\prod_{l=1}^{\infty}\frac{(1-\chi^{2l})^n}{(1-\gamma^{2l})}\right]. \end{aligned} \tag{3.2.14}$$

From this latter formula it is possible to appreciate entanglement equipartition between charge sectors with clarity as the dependence on charge number q is lost.

The even case (1)

In this second case we will go through very similar steps but this time with M being odd and the summation including only even indexes. Likewise:

$$\begin{aligned} \mathcal{Z}_n^{(1)}(\alpha) &= \prod_{m\geq 2}\left[(1-\xi_m)^{2n}+\xi_m^{2n}+(1-\xi_m)^n(\xi_m)^n 2\cos(\alpha)\right]\times\frac{1}{2^{n-1}}\cos\left(\frac{\alpha}{2}\right) = \\ &= \frac{1}{2^{n-1}}\cos\left(\frac{\alpha}{2}\right)\times\prod_{m\geq 2}\frac{[1+\chi^{nm}2\cos(\alpha)+\chi^{2nm}]}{(1+\chi^m)^{2n}} = \\ &= \frac{1}{2^{(n-1)}}\cos\left(\frac{\alpha}{2}\right)\prod_{l=1}^{\infty}\frac{(1+2\gamma^{2l}\cos(\alpha)+\gamma^{4l})}{(1+\chi^{2l})^{2n}}, \end{aligned} \tag{3.2.15}$$

in which, again, we used $\gamma=\chi^n$. Few differences can already be spotted comparing with Eq.(3.2.9) like the additional cosine factor in front and the exponents being indeed even. As a consequence we won't make use of the Jacobi theta function θ_3 but rather θ_2[38, (20.5.2)]:

$$\theta_2(z,s) = 2s^{\frac{1}{4}}\cos(z)\prod_{l=1}^{\infty}(1-s^{2l})(1+2s^{2l}\cos(2z)+s^{4l}), \tag{3.2.16}$$

thanks to which is possible to rephrase charge momenta equation as:

$$\begin{aligned} \mathcal{Z}_n^{(1)}(\alpha) &= \frac{2}{2^n}\frac{\gamma^{\frac{1}{4}}}{\gamma^{\frac{1}{4}}}\cos\left(\frac{\alpha}{2}\right)\prod_{l=1}^{\infty}\frac{(1-\gamma^{2n})}{(1-\gamma^{2n})}\frac{(1+2\gamma^{2l}\cos(\alpha)+\gamma^{4l})}{(1+\chi^{2l})^{2n}} = \\ &= \theta_2\Big(\frac{\alpha}{2},\gamma\Big)\frac{1}{2^n\gamma^{\frac{1}{4}}}\prod_{l=1}^{\infty}\frac{1}{(1-\chi^{2ln})(1+\chi^{2l})^{2n}} = \theta_2\Big(\frac{\alpha}{2},\gamma\Big)A_n^{(1)}. \end{aligned} \tag{3.2.17}$$

From there, to Fourier transform, one shall consider a second identity [38, (20.2.2)]:

$$\theta_2(z,s) = 2\sum_{l=0}^{\infty}s^{(l+\frac{1}{2})^2}\cos((2l+1)z) = \sum_{m\in\mathbb{Z}+\frac{1}{2}}s^{m^2}e^{i2mz}, \tag{3.2.18}$$

which comes helpful to derive:

$$Z_n^{(1)}(q) = A_n^{(1)}\gamma^{q^2} = A_n^{(1)}\chi^{nq^2}, \tag{3.2.19}$$

and in particular:

$$Z_1^{(1)}(q) = A_1^{(1)}\chi^{q^2} = \frac{1}{2\chi^{\frac{1}{4}}}\prod_{l=1}^{\infty}\frac{1}{(1-\chi^{2l})(1+\chi^{2l})^2}\chi^{q^2} = \frac{1}{\theta_2(0,\chi)}\chi^{q^2}. \tag{3.2.20}$$

As expected, $Z_1^{(1)}(q)$ is also gaussian and really mimics the odd FCS, Eq.(3.2.13), if not for θ_2 replacing θ_3. Plots of these distributions can be found in Fig.(3.8) for reference values of $\delta = 0.05$ and $\delta = 0.001$. As it can be observed, except for the odd FCS being related to integer charges and the even one to half-integers, the two of them basically trace back to the same gaussian for these parameters. This is a consequence of second and third Jacobi theta functions coinciding with an error $\propto 10^{-2}$ when their first argument is trivial and $\delta \propto 0.05$ or lower.

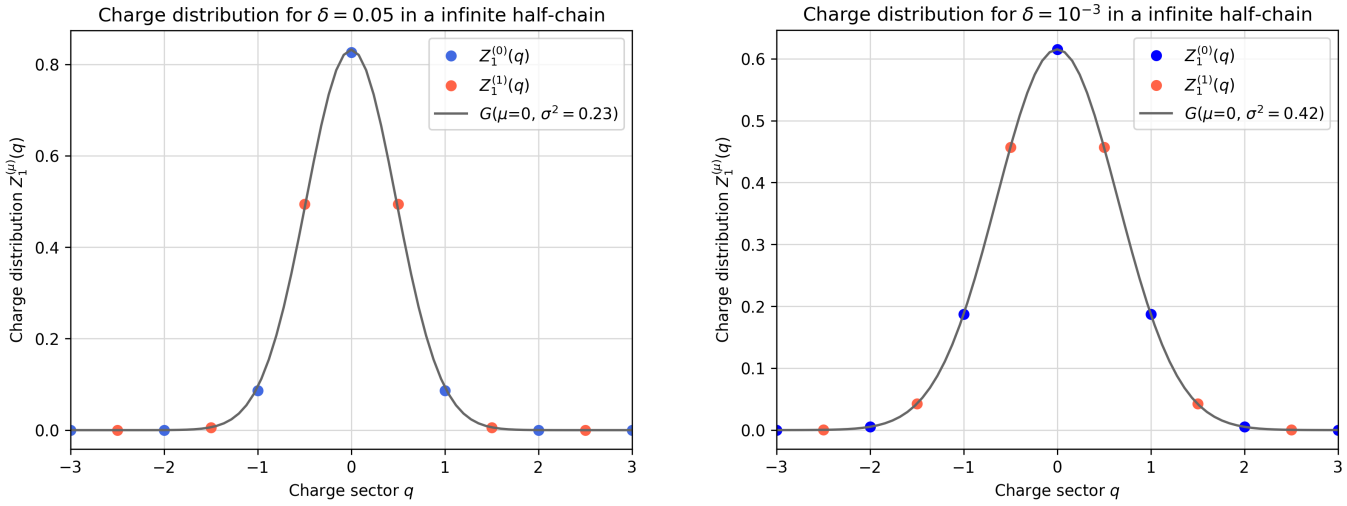

(a) $Z_1^{(0,1)}(q)$ for $\delta = 0.05$.

(b) $Z_1^{(0,1)}(q)$ for $\delta = 0.001$.

Fig. 3.8: Comparison between odd and even charge distributions for $\delta = 0.05$ and $\delta = 0.001$. Combining $Z_1^{(0)}$ defined for integer and $Z_1^{(1)}$ for half-integer charges q an overall unique gaussian fit can be performed as the two graphs show.

In the end, the explicit expression for symmetry resolved Rényi entropies is:

$$\begin{aligned} S_n^{(1)}(q) &= \frac{1}{1-n}\ln\left[\frac{A_n^{(1)}}{(A_1^{(1)})^n}\right] = \frac{1}{1-n}\ln\left[\frac{(2\chi^{\frac{1}{4}})^n}{2^n\gamma^{\frac{1}{4}}}\prod_{l=1}^{\infty}\frac{(1-\chi^{2l})^n(1+\chi^{2l})^{2n}}{(1-\chi^{2ln})(1+\chi^{2l})^{2n}}\right] = \\ &= \frac{1}{1-n}\ln\left[\prod_{l=1}^{\infty}\frac{(1-\chi^{2l})^n}{(1-\gamma^{2l})}\right]. \end{aligned} \tag{3.2.21}$$

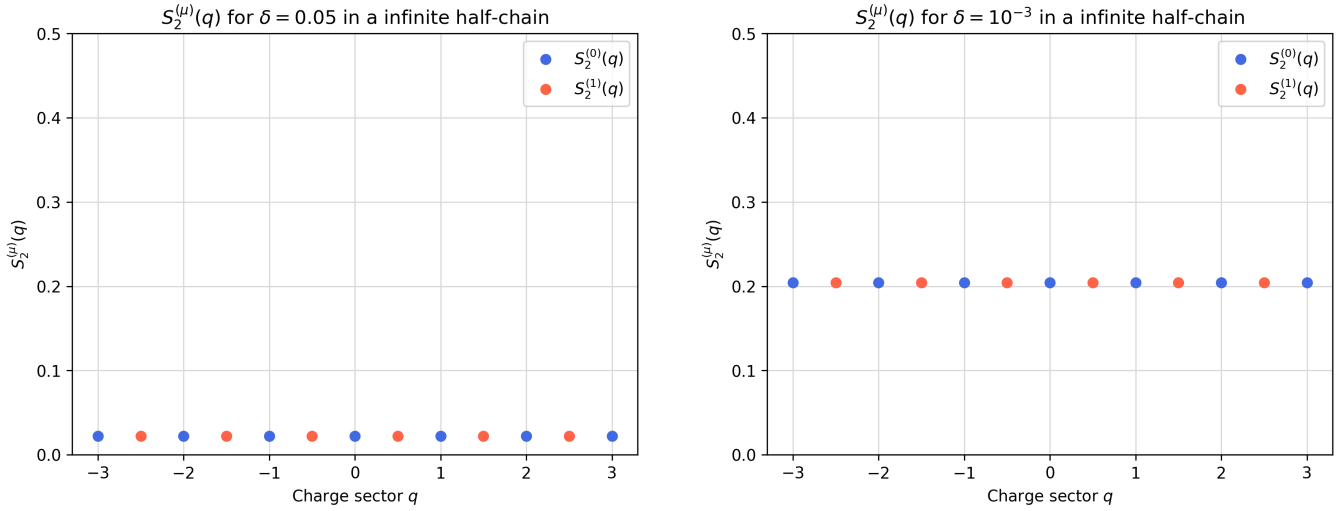

(a) $S_2^{(\mu)}(q)$ for $\delta = 0.05$.

(b) $S_2^{(\mu)}(q)$ for $\delta = 0.001$.

Fig. 3.9: $S_2^{(\mu)}(q)$ for $\delta = 0.05$ and $\delta = 0.001$. From each charge sectors we obtain the very same contributions, even comparing odd and even scenarios. For an infinite half-chain equipartition holds.

Again equipartition is present and, quite surprisingly, we recover the very same expression of the odd case, Eq.(3.2.14), id est $S_n^{(0)} = S_n^{(1)}$. In the interest of completeness, plots of $S_2^{(\mu)}(q)$ for $\delta = 0.05$ and $\delta = 0.001$ are provided in Fig.(3.9). Not much can be commented here as equipartition forces all points to lay at the same level, yet it can be notice we have a greater contribution from each sector as δ gets smaller.

3.2.2 SRRE in the limit of an infinite chain

Using the results of the previous sections it is finally possible to extend the analysis to the limit case for $M \to \infty$, id est for an infinite chain with double boundaries. In such setup the two edges of the interval will not interact with each other and the bi-partition can be thus studied as the union of two disjoint spectra for infinite half-chains. As seen before, 3 different scenarios enter the framework here, depending on where the edges are placed. One thus has to considered the usual three sets of entanglement eigenvalues combined: WW, SS and WS. According to those premises and reminding Eq.(3.1.4), one expects charged momenta to factorize as:

$$\mathcal{Z}_n^{(\mu,\nu)}(\alpha) = \mathcal{Z}_n^{(\mu)}(\alpha)\mathcal{Z}_n^{(\nu)}(\alpha), \tag{3.2.22}$$

with the indexes (μ, ν) for $\mu, \nu = 0, 1$ identifying the spectra listed. Next, after Fourier transform, one gets:

$$Z_n^{(\mu,\nu)}(q) = \sum_{q' \in \mathbb{Z}+\frac{\mu}{2}} Z_n^{(\mu)}(q') Z_n^{(\nu)}(q-q'), \tag{3.2.23}$$

with q' being integer or half integer depending on μ while q is integer if $\mu = \nu$ or half-integer vice versa. This latter can be eventually parametrized as $q \in \mathbb{Z} + \frac{(\mu-\nu)}{2}$. Eq.(3.2.23) is nothing but the discrete convolution over charge sectors of Z_n^μ and Z_n^ν. Plugging in their explicit expressions, Eqs.(3.2.12), (3.2.19), the above result can be rephrased in:

$$\begin{aligned} Z_n^{(\mu,\nu)}(q) &= A_n^{(\mu)} A_n^{(\nu)} \sum_{q' \in \mathbb{Z}+\frac{\mu}{2}} \chi^{nq'^2} \chi^{n(q-q')^2} = \\ &= A_n^{(\mu)} A_n^{(\nu)} \chi^{n\frac{q^2}{2}} \sum_{q' \in \mathbb{Z}+\frac{\mu}{2}} \chi^{2n(q'-\frac{q}{2})^2}. \end{aligned} \tag{3.2.24}$$

At this point the attention must be drawn at the summation:

$$F_n^{(\mu,\nu)}(q) = \sum_{q' \in \mathbb{Z}+\frac{\mu}{2}} \chi^{2n(q'-\frac{q}{2})^2}, \tag{3.2.25}$$

which is a function showing different behaviours depending on the indexes μ, ν. In the interest of clarity, solving for the parametrization:

$$\begin{cases} q' = s + \frac{\mu}{2}, \\ q = t + \frac{\mu-\nu}{2}, \end{cases}$$

Eq.(3.2.25) becomes,

- for $\mu = \nu$:

$$F_n^{(\mu,\mu)}(t) = \sum_{s,t \in \mathbb{Z}} \chi^{2n(s+\frac{\mu-t}{2})^2} = \begin{cases} \sum_{p \in \mathbb{Z}} \chi^{2np^2} = \theta_3(0, \chi^{2n}) & \text{if } t \mod 2 = \mu, \\ \sum_{p \in \mathbb{Z}+\frac{1}{2}} \chi^{2np^2} = \theta_2(0, \chi^{2n}) & \text{if } t \mod 2 \neq \mu, \end{cases} \tag{3.2.26}$$

- for $\mu \neq \nu$:

$$\begin{aligned} F_n^{(\mu,\nu)}(t \pm \frac{1}{2}) &= \sum_{s \in \mathbb{Z}} \chi^{2n(s+\frac{\mu+t}{2} \pm \frac{1}{4})^2} = \frac{1}{2}\Bigg[\sum_{p \in \mathbb{Z}+\frac{1}{4}} \chi^{2np^2} + \sum_{p \in \mathbb{Z}+\frac{3}{4}} \chi^{2np^2} \Bigg] = \\ &= \frac{1}{2}\Bigg[\sum_{p \in \mathbb{Z}/4} \chi^{2np^2} - \sum_{p \in \mathbb{Z}} \chi^{2np^2} - \sum_{p \in \mathbb{Z}+\frac{1}{2}} \chi^{2np^2} \Bigg] = \\ &= \frac{1}{2}\Big[\theta_3(0, \chi^{\frac{n}{8}}) - \theta_3(0, \chi^{2n}) - \theta_2(0, \chi^{2n}) \Big]. \end{aligned} \tag{3.2.27}$$

In the former case $F_n^{(\mu,\nu)}(q)$ oscillates between two Jacobi theta functions with period 2 while in the latter it stays constant for any value of q.

Using the above results, symmetry resolved Rényi entropies can be recasted, scenario by scenario, as follows:

1. Weak-Strong cuts (WS) or vice versa, $\mu \neq \nu$:

$$
\begin{aligned}
S_n^{(\mu,\nu)}(q) &= \frac{1}{1-n}\ln\frac{Z_n^{(\mu,\nu)}(q)}{\left[Z_1^{(\mu,\nu)}(q)\right]^n} = \frac{1}{1-n}\ln\frac{A_n^{(0)}A_n^{(1)}F_n^{(\mu,\nu)}(q)}{\left[A_1^{(0)}A_1^{(1)}F_1^{(\mu,\nu)}(q)\right]^n} = \\
&= \frac{1}{1-n}\left[\ln\frac{A_n^{(0)}}{[A_1^{(0)}]^n} + \ln\frac{A_n^{(1)}}{[A_1^{(1)}]^n} + \ln\frac{F_n^{(\mu,\nu)}(q)}{\left[F_1^{(\mu,\nu)}(q)\right]^n}\right] \\
&= S_n^{(0)} + S_n^{(1)} + \frac{1}{1-n}\ln\left[2^{(n-1)}\frac{\theta_3(0,\chi^{\frac{n}{8}}) - \theta_3(0,\chi^{2n}) - \theta_2(0,\chi^{2n})}{\left[\theta_3(0,\chi^{\frac{1}{8}}) - \theta_3(0,\chi^{2}) - \theta_2(0,\chi^{2})\right]^n}\right].
\end{aligned}
\tag{3.2.28}
$$

2. Weak-Weak cuts (WW), $\mu = \nu = 0$:

$$
\begin{aligned}
S_n^{(0,0)}(q) &= \frac{1}{1-n}\ln\frac{Z_n^{(0,0)}(q)}{\left[Z_1^{(0,0)}(q)\right]^n} = \frac{1}{1-n}\ln\frac{[A_n^{(0)}]^2F_n^{(0,0)}(q)}{\left[A_1^{(0)}\right]^{2n}\left[F_1^{(0,0)}(q)\right]^n} = \\
&= 2S_n^{(0)}(q) + \begin{cases} \frac{1}{1-n}\ln\left[2^{n-1}\frac{\theta_3(0,\chi^{2n})}{[\theta_3(0,\chi^2)]^n}\right] & \textit{if: } q \mod 2 = 0, \\ \frac{1}{1-n}\ln\left[2^{n-1}\frac{\theta_2(0,\chi^{2n})}{[\theta_2(0,\chi^2)]^n}\right] & \textit{if: } q \mod 2 = 1. \end{cases}
\end{aligned}
\tag{3.2.29}
$$

3. Strong-Strong cuts (SS), $\mu = \nu = 1$:

$$
\begin{aligned}
S_n^{(1,1)}(q) &= \frac{1}{1-n}\ln\frac{Z_n^{(1,1)}(q)}{\left[Z_1^{(1,1)}(q)\right]^n} = \frac{1}{1-n}\ln\frac{[A_n^{(1)}]^2F_n^{(1,1)}(q)}{\left[A_1^{(1)}\right]^{2n}\left[F_1^{(11)}(q)\right]^n} = \\
&= 2S_n^{(1)}(q) + \begin{cases} \frac{1}{1-n}\ln\left[2^{n-1}\frac{\theta_3(0,\chi^{2n})}{[\theta_3(0,\chi^2)]^n}\right] & \textit{if: } q \mod 2 = 1 \\ \frac{1}{1-n}\ln\left[2^{n-1}\frac{\theta_2(0,\chi^{2n})}{[\theta_2(0,\chi^2)]^n}\right] & \textit{if: } q \mod 2 = 0 \end{cases}
\end{aligned}
\tag{3.2.30}
$$

Despite their unfriendly shapes, above formulae describe a rather simple framework: for mixed cuts still we witness exact equipartition between charge sectors while, in the homogenous scenarios, Rényi entropies oscillate with opposite phases, *de facto* breaking pure equipartition in favor of an oscillating pattern. The shift between WW and SS can be eventually encoded writing $S_n^{(0,0)}(q) = S_n^{(1,1)}(q+1)$.

To not break continuity with past figures, graphs of second order SRRE can be found in Fig.(3.10) for $\delta = 0.05$ and $\delta = 0.001$. Intuitively they can be thought as the limit cases for $N \to \infty$ of Figs.(3.4),(3.5).

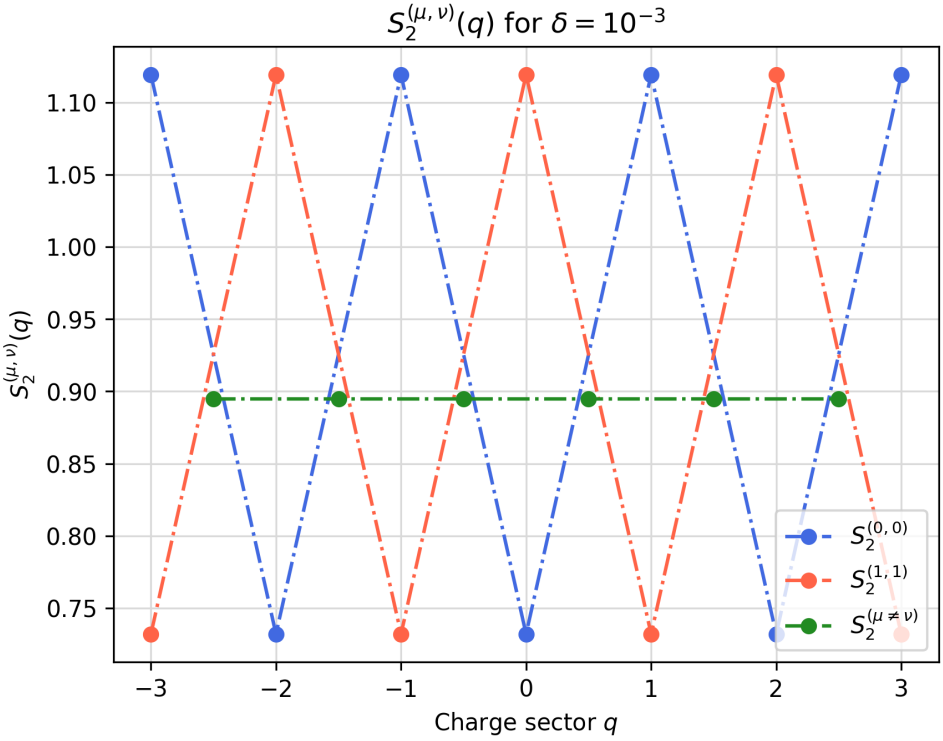

(a) $S_2^{(\mu,\nu)}(q)$ for $\delta = 0.05$.

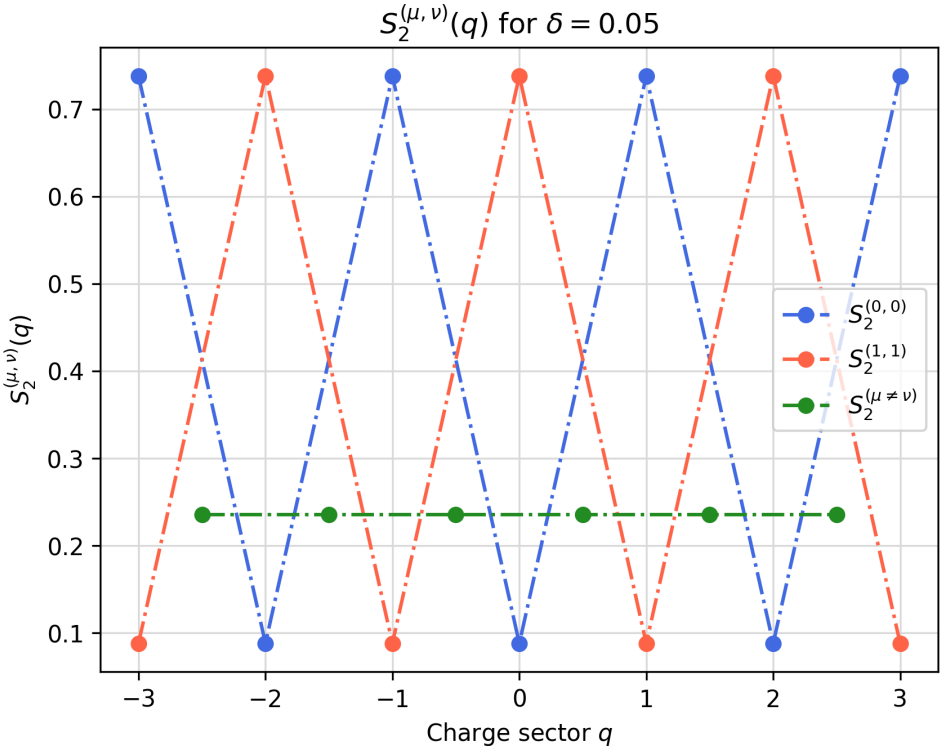

(b) $S_2^{(\mu,\nu)}(q)$ for $\delta = 0.001$.

Fig. 3.10: $S_2^{(\mu,\nu)}(q)$ for $\delta = 0.05$ and $\delta = 0.001$. This time equipartition holds only for the mixed scenario when $\mu \neq \nu$, in the other setup it breaks in favor of an oscillating behaviour.

3.3 SRRE in generalized free fermion chain

Following the approach used for the SSH model it would be really interesting to extend predictions regarding SRRE to even more generic models. Let me thus use this section to present some preliminary results which may serve in future for such purpose.

Hamiltonians for free fermion chains can be formulated, excluding on-site potentials, as:

$$\hat{H} = \sum_{m,n} \sum_{\alpha,\beta} t_{m,n}^{\alpha,\beta} \, c_m^{\alpha\,\dagger} \, c_n^{\beta} \tag{3.3.1}$$

with m, n being cell indexes and α, β sublattice indexes. In the finite scenario we may assume $m, n \in [0, N-1]$ and $\alpha, \beta \in [0, S-1]$ with N size of the chain and S size of the cells. Considering PBC the system becomes translational invariant: $t_{m,n}^{\alpha,\beta} \to t_{(m-n)}^{\alpha,\beta}$, meaning it depends only on cell distance, and it is convenient to move to momentum space. Replacing the usual definitions for plane waves one is left with:

$$\hat{H} = \sum_{q} \sum_{\alpha,\beta} \tilde{t}_q^{\alpha,\beta} \, \tilde{c}_q^{\alpha\,\dagger} \, \tilde{c}_q^{\beta}, \tag{3.3.2}$$

for:

$$\tilde{t}_q^{\alpha,\beta} = \sum_{p} t_p^{\alpha\,\beta} e^{ik_q p}. \tag{3.3.3}$$

As for the SSH model, the problem is still not fully diagonalized but it is already possible to derive the full energy spectrum analyzing each $\tilde{t}_q^{\alpha,\beta}$.

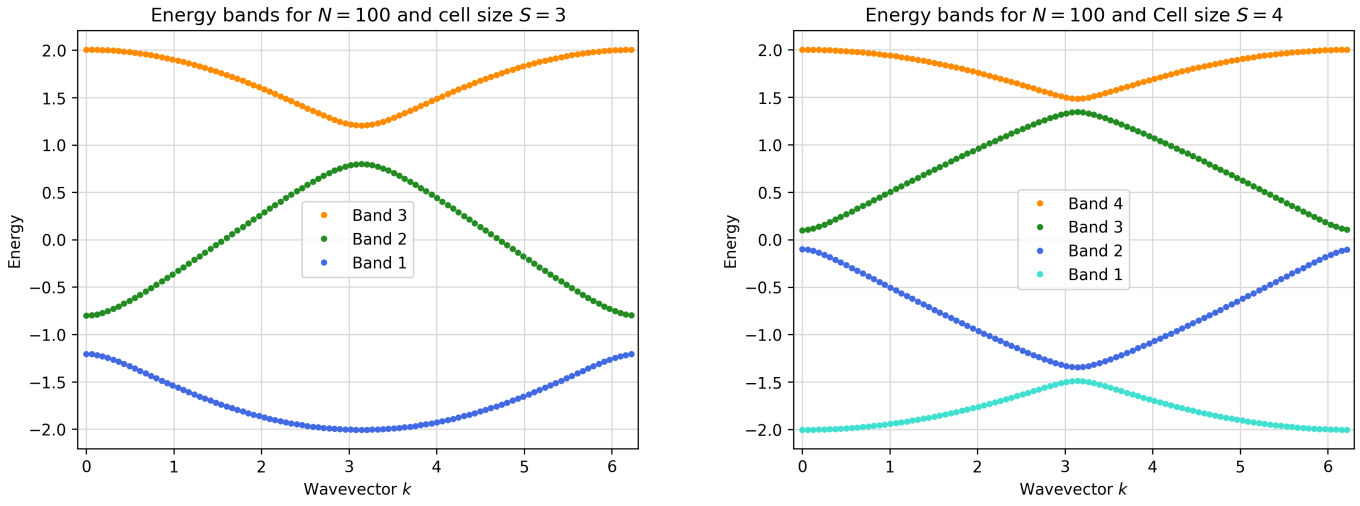

(a) Energy bands for $S = 3$.

(b) Energy bands for $S = 4$.

Fig. 3.11: Energy spectra for more general free fermion chains. In the present case two examples for $S = 3$ and $S = 4$ are considered.

By changing the parameters inside $\tilde{t}_q^{\alpha,\beta}$, a large multitude of different spectra can be

created with the total number of bands always matching the cell size S. In the interest of clarity two simple examples can be observed in Fig.(3.11). Within this general framework, the definition of the groundstate also opens to many possibilities as one can even choose the amount of bands to be filled. According to this choice, the computation of correlation matrix elements will need the proper adjustments.

The full diagonal form of $\hat{H}$ can be then achieved, easily or not, following the same scheme discussed for the SSH model and, with the new operators found, one can derive the corresponding correlation matrix C. Note however, that the various simplifications will not apply this time as the system is now completely different. Subsequently, extracted the eigenvalues of its reduced version $C_{\mathcal{A}}$, one can again investigate second order SRRE which, in this case, will outline a way richer scenario. Using this general formulation in fact, an indefinite number of different links might be inserted in the chain causing the presence of a large multitude of possible boundary combinations. In addition to that, technical problems arise as in this framework there are still no methods to compute analytically the eigenvalues for subsystems of infinite sizes. As a consequence, to look for sharp patterns we are forced to simulate very large systems and this generally takes an unreasonable amount of time.

Sticking to small subsystems, few simulations has been performed with the most interesting results plotted in Fig.(3.12). Even though they refer to two different systems both seem to suggest the presence of patterns regarding the distribution of entanglement. Specifically Fig.(3.12(a)) refers to a system with cells of size $S = 3$ featuring three alternating hopping parameters: $t_1 = 0.9$, $t_2 = 1$ and $t_3 = 1.1$. In the picture, $S_2(q)$ is plotted considering always the same boundary combination but increasing the subsystem size. As it can be observed, with the number of cells N growing, the distribution seems to flatten. Speaking then of Fig.(3.12(b)), these are the results for a system with cells of size $S = 4$ and hopping parameters $t_1 = 0.9$, $t_2 = 1$, $t_3 = 1.1$ and $t_4 = 1.2$. In this case N is fixed and SRREs are computed for different boundary combinations. Looking at the picture some clear patterns already show up.

All in all, simulations for finite subsystems are encouraging, but to derive exact formulae further methods are needed.

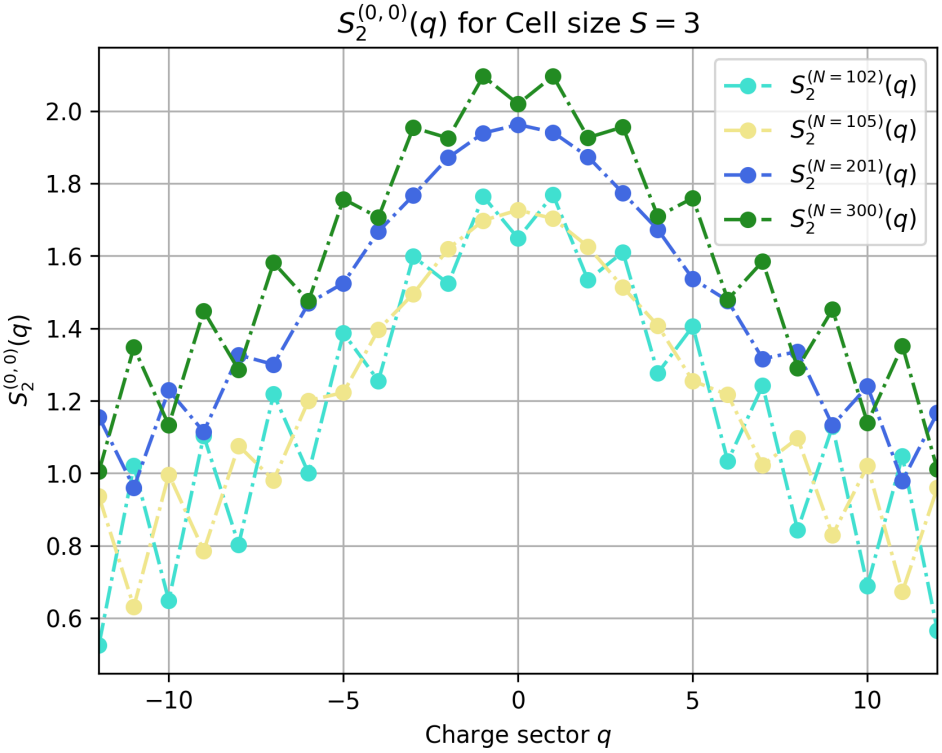

(a) $S_2(q)$ distribution for $S = 3$ and N variable.

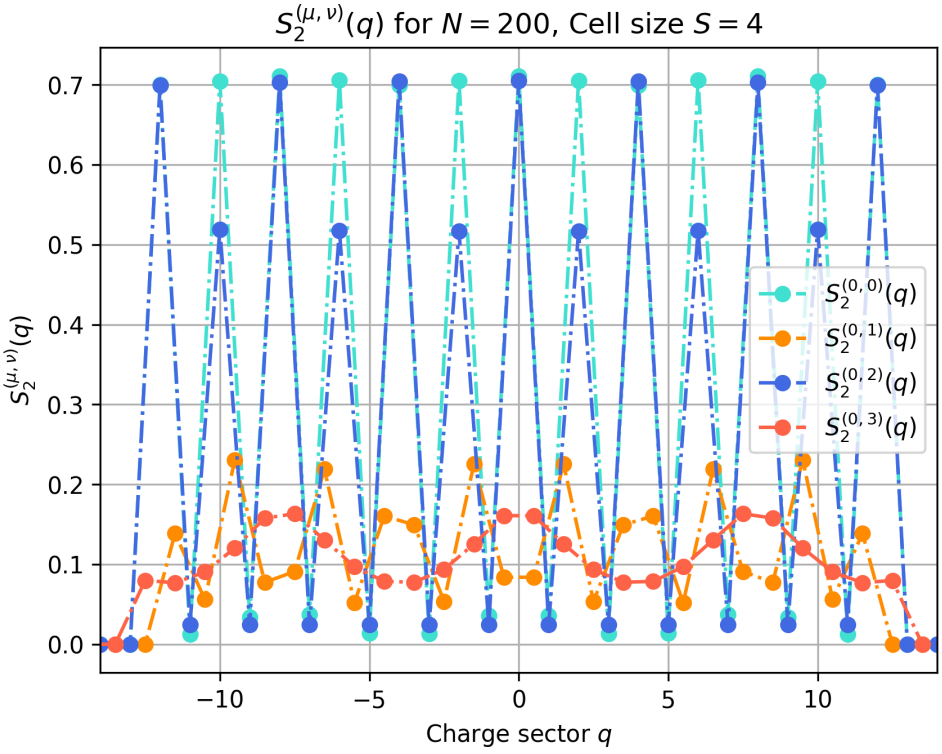

(b) $S_2(q)$ distribution for $S = 4$ with different boundaries.

Fig. 3.12: Second order SRRE distributions for two different systems with $S = 3$ and $S = 4$. In **a)** $S_2(q)$ is studied keeping the boundaries on fixed links while varying the subsystem size. In **b)** instead the size has been kept constant while boundaries has been change.

Conclusions

In this thesis entanglement entropies in the hopping and the SSH models are investigated. Using the correlation function method, the entanglement content of the two free fermion models has been computed. In this regard, explicit formulae for the correlation matrix elements are provided throughout this elaborate as key ingredients for the creation of a reliable code. This is the case of Eqs.(2.1.9), (2.1.11), (2.2.17) and (2.2.19). With the support of numerical simulations, the main predictions coming from CFT are perfectly matched for the hopping model with Eqs.(1.3.22), (1.3.21) tracing exactly the data recorded in Figs.(2.3(b)), (2.6). Regarding the SSH model interesting phenomena are discussed, namely the saturation and the split in multiple branches of Von Neumann entanglement entropy. Respectively, they can be observed in Figs.(2.9(a)), (2.9(b)) for a finite chain, in Figs.(2.11(a))-(2.11(b)), (2.12) in the infinite case.

Moving to the study of second order SRRE in SSH model and starting from the finite scenario, numerical simulations allowed to esteem and plot the entanglement content per charge sector. Results are in Figs.(3.4), (3.5). Their analysis highlighted the presence of recurrent patterns, possibly having a precise behaviour in the limit for the size of the partition going to infinite. This is what inspired to include in the investigation also infinite subsystems, specifically the infinite half-chain and the infinite chain. Outcomes for the former are collected in Fig.(3.9) and feature exact equipartition. For the latter, results can be observed in Fig.(3.10). As claimed, this scenario is richer and characterized by the appearance of sharp patterns whose shape is determined by Eqs.(3.2.28), (3.2.29) and (3.2.30). In this case equipartition holds only for mixed boundaries and it is lost otherwise.

Drawing the attention to future outlooks, it would be interesting to be able to characterize SRRE even in more generic free fermion chains. Fig.(3.12) seems to be suggest the existence of such patterns, though it has been not possible to exactly predict them. Another direction could be that of computing SRRE for *graphene* which can be modelled as an ensemble of SSH models[39].

Appendix A

Simplification of correlation matrix element

In the interest of clarity let me rewrite the starting equation:

$$\begin{aligned} C_{mn,AB} = -\frac{1}{2N}\sum_{q=0}^{N-1} e^{-ik(q)[m-n]}\sqrt{\frac{t_1+t_2\,e^{ik(q)}}{t_1+t_2\,e^{-ik(q)}}} \\ \xrightarrow[N\to\infty]{q\to k(q)} \; -\int_{-\pi}^{\pi}\frac{dk}{4\pi}e^{-ik(m-n)}\sqrt{\frac{t_1+t_2e^{ik}}{t_1+t_2e^{-ik}}}. \end{aligned} \tag{A.0.1}$$

Recalling the parametrization for t_1, t_2 in Eq.(2.2.9), with $\delta > 0$ being half the gap, and replacing k with the complex variable $z = e^{-ik}$, the above equation can be rephrased as:

$$\begin{aligned} C_{mn,AB} &= -\int_{-\pi}^{\pi}\frac{dk}{4\pi}e^{-ik(m-n)}\sqrt{\frac{1+\epsilon e^{ik}}{1+\epsilon e^{-ik}}} = \quad \textit{for:}\;\; \epsilon = \frac{1-\delta}{1+\delta} \\ &= \oint_{C_1}\frac{dz}{4\pi i}z^{(m-n)-1}\sqrt{\frac{1+\epsilon z^{-1}}{1+\epsilon z}} = \oint_{C_1}\frac{dz}{4\pi i}z^{(m-n)-1}f(z). \end{aligned} \tag{A.0.2}$$

Borrowing lexicon from quantum field theories one might be more familiar with the notation by referring to the above expression as the propagator between the m^{th} and n^{th} cells:

$$C_{mn,AB} = D(m-n), \tag{A.0.3}$$

At this point, expanding $f(z) = \sum_{r\in\mathbb{Z}} a_r z^r$ and considering *Cauchy's integral formula*, the problem reduces, up to constants, to the esteem of the $(n-m)^{th}$ Laurent coefficient of $f(z)$:

$$D(m-n) = \oint_{C_1}\frac{dz}{4\pi i}\,\frac{1}{z}\Big(\sum_{r=-\infty}^{\infty} a_r z^{r+(m-n)}\Big) = \frac{1}{2}a_{n-m}. \tag{A.0.4}$$

In details, inside the annulus $\epsilon < |z| < \epsilon^{-1}$, one can write:

$$\begin{aligned} f(z) &= (1+\epsilon z^{-1})^{\frac{1}{2}}(1+\epsilon z)^{-\frac{1}{2}}\left(1+\frac{1}{2}\epsilon z^{-1}-\frac{1}{8}\epsilon^2 z^{-2}+\cdots\right)\left(1-\frac{1}{2}\epsilon z+\frac{3}{8}\epsilon^2 z^2\cdots\right) = \\ &= \left[\sum_{q\geq 0}\binom{\frac{1}{2}}{q}\epsilon^q z^{-q}\right]\left[\sum_{p\geq 0}\binom{-\frac{1}{2}}{p}\epsilon^p z^p\right] \equiv \sum_{r=-\infty}^{\infty} a_r z^r, \end{aligned} \tag{A.0.5}$$

with the binomial coefficient for real numbers defined after the identity:

$$\binom{\alpha}{\beta} = \frac{\Gamma(\alpha+1)}{\Gamma(\beta+1)\Gamma(\alpha-\beta+1)}. \tag{A.0.6}$$

The explicit expression for the r^{th} Laurent coefficient is then given by the combination of all terms such that $p-q=r$. Indeed, replacing $p=q+r$ while keeping $p\geq 0$ leads to:

$$\begin{aligned} a_r &= \left[\sum_{q\geq 0}\binom{\frac{1}{2}}{q}\epsilon^q\right]\left[\sum_{q\geq -r}\binom{-\frac{1}{2}}{r+q}\epsilon^{q+r}\right] = \sum_{q\geq \max\{0,-r\}}\left[\binom{\frac{1}{2}}{q}\binom{-\frac{1}{2}}{r+q}\epsilon^{2q+r}\right] = \\ &= \begin{cases} \textit{if } r>0: & \sum_{q\geq 0}\left[\binom{\frac{1}{2}}{q}\binom{-\frac{1}{2}}{r+q}\epsilon^{2q+r}\right] = \epsilon^r\binom{-\frac{1}{2}}{r}\,{}_2F_1\Big(-\frac{1}{2},\frac{1}{2}+r,1+r,\epsilon^2\Big), \\ \textit{if } r<0: & \sum_{q\geq -r}\left[\binom{\frac{1}{2}}{q}\binom{-\frac{1}{2}}{r+q}\epsilon^{2q+r}\right] = \epsilon^{-r}\binom{\frac{1}{2}}{-r}\,{}_2F_1\Big(\frac{1}{2},-\frac{1}{2}-r,1-r,\epsilon^2\Big), \end{cases} \end{aligned} \tag{A.0.7}$$

with ${}_2F_1$ being the hypergeometric function[38][40], defined as:

$${}_2F_1(\alpha,\beta,\gamma,z) \equiv F(\alpha,\beta,\gamma,z) = \sum_{n=0}^{\infty}\frac{(\alpha)_n(\beta)_n}{\Gamma(\gamma+n)n!}z^n, \tag{A.0.8}$$

and $(\alpha)_n$ being the Pochhammer symbol:

$$(\alpha)_n = \alpha(\alpha+1)\cdots(\alpha+n-1). \tag{A.0.9}$$

In Eqs.(A.0.7),(A.0.8), the presence of binomial coefficients, Pochhammer symbols, gamma functions and factorials must be handled very carefully when it comes to coding as series of products can easily lead to overflow errors. To avoid such contingency, both the binomial coefficients and the hypergeometrics function must be factorized properly when M grows in magnitude. In the former case it is enough to compute the series as:

$$\binom{\mp 0.5}{r} = \frac{\mp 0.5(\mp 0.5-1)(\cdots)(\mp 0.5-r+1)}{r!} = \prod_{i=0}^{r-1}\frac{\mp 0.5-i}{i+1}, \tag{A.0.10}$$

obtaining two convergent sequences. In the latter it is convenient to use the integral representation of the hypergeometric function [38, (15.6.1)]:

$$F(\alpha,\beta,\gamma,z) = \frac{\Gamma(\gamma)}{\Gamma(\beta)\Gamma(\gamma-\beta)}\int_0^1 \frac{t^{\beta-1}\,(1-t)^{\gamma-\beta-1}}{(1-zt)^{\alpha}}dt, \tag{A.0.11}$$

for which sources of overflow condense as a fraction of gamma functions in front of the integral. At this point, it is possible to reabsorb them as follows. Replacing the definitions of their arguments and considering:

$$\Gamma(z+1) = z\Gamma(z), \tag{A.0.12}$$

formula (A.0.11) can be reduced to:

$$F(\alpha,\beta,\gamma,z) = \begin{cases} \textit{if: } r>0 & \frac{\Gamma(1+r)}{\Gamma(\frac{1}{2}+r)\Gamma(\frac{1}{2})} \\ \textit{if: } r<0 & \frac{\Gamma(1-r)}{\Gamma(-\frac{1}{2}-r)\Gamma(\frac{3}{2})} \end{cases} \times \int_0^1 \frac{t^{\beta-1}\,(1-t)^{\gamma-\beta-1}}{(1-zt)^{\alpha}} dt = \\ = \begin{cases} \frac{\Delta_+}{\Gamma(\frac{1}{2})^2} \\ \frac{\Delta_-}{\Gamma(-\frac{1}{2})\Gamma(\frac{3}{2})} \end{cases} \times \int_0^1 \frac{t^{\beta-1}\,(1-t)^{\gamma-\beta-1}}{(1-zt)^{\alpha}} dt, \tag{A.0.13}$$

with:

$$\Delta_+ = \prod_{n=1}^{r} \frac{n}{n-\frac{1}{2}}, \qquad \Delta_- = \prod_{n=1}^{|r|} \frac{n}{n-\frac{3}{2}}. \tag{A.0.14}$$

Note that $\Delta_\pm$ are both divergent series, however their growth is so slow that there is no risk of overflows for systems of sizes $N \approx 10^3, 10^4$. All in all, one ends up with:

$$D(m-n) \equiv D(-r) = \frac{1}{2}a_r = \begin{cases} \frac{\epsilon^r}{2}\binom{-\frac{1}{2}}{r} \frac{\Delta_+}{\Gamma(\frac{1}{2})^2} \int_0^1 dt\, \frac{t^{r-\frac{1}{2}}\,(1-t)^{-\frac{1}{2}}}{(1-zt)^{-\frac{1}{2}}} & \textit{if: } r>0, \\ \frac{\epsilon^{-r}}{2}\binom{\frac{1}{2}}{-r} \frac{\Delta}{\Gamma(-\frac{1}{2})\Gamma(\frac{3}{2})} \int_0^1 dt\, \frac{t^{-r-\frac{3}{2}}\,(1-t)^{\frac{1}{2}}}{(1-zt)^{\frac{1}{2}}} & \textit{if: } r<0. \end{cases} \tag{A.0.15}$$

The above equation is the final result we were looking for. Still, before concluding this appendix, let me discuss here an additional consistency check that has been carried out as it involves hypergeometric functions. This consisted in testing the above formulae for $\delta = 0$ expecting to recover the same reduced correlation matrix of a non staggered hopping model. In this limit $\epsilon, z \to 1$ and one can thus take advantage of a simplified version of the hypergeometric function [38, (15.4.20)]:

$$F(\alpha,\beta,\gamma,1) = \frac{\Gamma(\gamma)\Gamma(\gamma-\alpha-\beta)}{\Gamma(\gamma-\alpha)\Gamma(\gamma-\beta)}. \tag{A.0.16}$$

to lighten the code. Results were compatible in this sense.

Bibliography

[1] E. Schrödinger. "Die gegenwärtige Situation in der Quantenmechanik". In: *Naturwissenschaften* 23.48 (Nov. 1935), pp. 807–812. DOI: 10.1007/BF01491891.

[2] A. Einstein, B. Podolsky, and N. Rosen. "Can Quantum-Mechanical Description of Physical Reality Be Considered Complete?" In: *Phys. Rev.* 47 (10 May 1935), pp. 777–780. DOI: 10.1103/PhysRev.47.777.

[3] A. Einstein, M. Born, and H. Born. *The Born-Einstein Letters: Correspondence Between Albert Einstein and Max and Hedwig Born from 1916-1955, with Commentaries by Max Born*. Macmillan, 1971. ISBN: 9780333112670.

[4] J. S. Bell. "On the Einstein-Podolsky-Rosen paradox". In: *Physics Physique Fizika* 1 (1964), pp. 195–200. DOI: 10.1103/PhysicsPhysiqueFizika.1.195.

[5] Christoph Holzhey, Finn Larsen, and Frank Wilczek. "Geometric and renormalized entropy in conformal field theory". In: *Nuclear Physics B* 424.3 (Aug. 1994), pp. 443–467. DOI: 10.1016/0550-3213(94)90402-2.

[6] Mark Srednicki. "Entropy and area". In: *Physical Review Letters* 71.5 (Aug. 1993), pp. 666–669. DOI: 10.1103/physrevlett.71.666.

[7] Charles H Bennett and David P DiVincenzo. "Quantum information and computation". In: *nature* 404.6775 (2000), pp. 247–255.

[8] Michael A. Nielsen and Isaac L. Chuang. *Quantum Computation and Quantum Information: 10th Anniversary Edition*. Cambridge University Press, 2010. DOI: 10.1017/CBO9780511976667.

[9] Luigi Amico et al. "Entanglement in many-body systems". In: *Rev. Mod. Phys.* 80 (2 May 2008), pp. 517–576. DOI: 10.1103/RevModPhys.80.517.

[10] Guifré Vidal. "Entanglement monotones". In: *Journal of Modern Optics* 47.2-3 (Feb. 2000), pp. 355–376. DOI: 10.1080/09500340008244048.

[11] Karol Zyczkowski and Ingemar Bengtsson. *An Introduction to Quantum Entanglement: a Geometric Approach*. 2006. arXiv: quant-ph/0606228 [quant-ph].

[12] J. L. Cardya. "Entanglement entropy in extended quantum systems". In: *The European Physical Journal B* 64.3-4 (Mar. 2008), pp. 321–326. DOI: 10.1140/epjb/e2008-00102-5.

[13] J. Eisert, M. Cramer, and M. B. Plenio. "Colloquium: Area laws for the entanglement entropy". In: *Rev. Mod. Phys.* 82 (1 Feb. 2010), pp. 277–306. DOI: 10.1103/RevModPhys.82.277.

[14] Pasquale Calabrese and John Cardy. "Entanglement entropy and quantum field theory". In: *Journal of Statistical Mechanics: Theory and Experiment* 2004.06 (June 2004), P06002. DOI: 10.1088/1742-5468/2004/06/p06002.

[15] Moshe Goldstein and Eran Sela. "Symmetry-Resolved Entanglement in Many-Body Systems". In: *Physical Review Letters* 120.20 (May 2018). DOI: 10.1103/physrevlett.120.200602.

[16] Luca Capizzi, Paola Ruggiero, and Pasquale Calabrese. "Symmetry resolved entanglement entropy of excited states in a CFT". In: *Journal of Statistical Mechanics: Theory and Experiment* 2020.7 (July 2020), p. 073101. DOI: 10.1088/1742-5468/ab96b6.

[17] J. C. Xavier, F. C. Alcaraz, and G. Sierra. "Equipartition of the entanglement entropy". In: *Phys. Rev. B* 98 (4 July 2018), p. 041106. DOI: 10.1103/PhysRevB.98.041106.

[18] Martin B. Plenio and S. Virmani. *An introduction to entanglement measures*. 2006. arXiv: quant-ph/0504163 [quant-ph].

[19] Erhard Schmidt. "Zur Theorie der linearen und nichtlinearen Integralgleichungen. I. Teil: Entwicklung willkürlicher Funktionen nach Systemen vorgeschriebener". In: *Mathematische Annalen* 63 (1907), pp. 433–476.

[20] Hui Li and F. D. M. Haldane. "Entanglement Spectrum as a Generalization of Entanglement Entropy: Identification of Topological Order in Non-Abelian Fractional Quantum Hall Effect States". In: *Phys. Rev. Lett.* 101 (1 July 2008), p. 010504. DOI: 10.1103/PhysRevLett.101.010504.

[21] Ingo Peschel and Viktor Eisler. "Reduced density matrices and entanglement entropy in free lattice models". In: *Journal of Physics A: Mathematical and Theoretical* 42.50 (Dec. 2009), p. 504003. DOI: 10.1088/1751-8113/42/50/504003.

[22] Ingo Peschel. "Special Review: Entanglement in Solvable Many-Particle Models". In: *Brazilian Journal of Physics* 42.3-4 (Mar. 2012), pp. 267–291. DOI: 10.1007/s13538-012-0074-1.

[23] Ingo Peschel. "Calculation of reduced density matrices from correlation functions". In: *Journal of Physics A: Mathematical and General* 36.14 (Mar. 2003), pp. L205–L208. DOI: 10.1088/0305-4470/36/14/101.

[24] Luca Guido Molinari. *Notes on Wick's theorem in many-body theory*. 2017. arXiv: 1710.09248 [math-ph].

[25] Ingo Peschel. "On the reduced density matrix for a chain of free electrons". In: *Journal of Statistical Mechanics: Theory and Experiment* 2004.06 (June 2004), P06004. DOI: 10.1088/1742-5468/2004/06/p06004.

[26] Pasquale Calabrese and John Cardy. *Entanglement entropy and quantum field theory: a non-technical introduction*. 2005. arXiv: quant-ph/0505193 [quant-ph].

[27] Pasquale Calabrese and John Cardy. "Entanglement entropy and conformal field theory". In: *Journal of Physics A: Mathematical and Theoretical* 42.50 (Dec. 2009), p. 504005. DOI: 10.1088/1751-8113/42/50/504005.

[28] J. L. Cardy, O. A. Castro-Alvaredo, and B. Doyon. "Form Factors of Branch-Point Twist Fields in Quantum Integrable Models and Entanglement Entropy". In: *Journal of Statistical Physics* 130.1 (Oct. 2007), pp. 129–168. DOI: 10.1007/s10955-007-9422-x.

[29] Alexander A Belavin, Alexander M Polyakov, and Alexander B Zamolodchikov. "Infinite conformal symmetry in two-dimensional quantum field theory". In: *Nuclear Physics B* 241.2 (1984), pp. 333–380.

[30] P. Di Francesco, P. Mathieu, and D. Senechal. *Conformal Field Theory*. Graduate Texts in Contemporary Physics. New York: Springer-Verlag, 1997. ISBN: 978-0-387-94785-3, 978-1-4612-7475-9. DOI: 10.1007/978-1-4612-2256-9.

[31] Steven H. Simon. *The Oxford Solid State Basics / Steven H. Simon.* eng. First edition. Oxford: Oxford University Press, 2013. ISBN: 9780191502101.

[32] János K. Asbóth, László Oroszlány, and András Pályi. *A Short Course on Topological Insulators*. Springer International Publishing, 2016. DOI: 10.1007/978-3-319-25607-8.

[33] Giuseppe Mussardo. *Statistical field theory: an introduction to exactly solved models in statistical physics; 1st ed.* Oxford graduate texts. New York, NY: Oxford Univ. Press, 2010.

[34] Leonid S. Levitov, Hyunwoo Lee, and Gordey B. Lesovik. "Electron counting statistics and coherent states of electric current". In: *Journal of Mathematical Physics* 37.10 (Oct. 1996), pp. 4845–4866. ISSN: 0022-2488. DOI: 10.1063/1.531672.

[35] Blagoje Oblak, Nicolas Regnault, and Benoit Estienne. "Equipartition of entanglement in quantum Hall states". In: *Physical Review B* 105.11 (Mar. 2022). DOI: 10.1103/physrevb.105.115131.

[36] Alexander Lukin et al. "Probing entanglement in a many-body–localized system". In: *Science* 364.6437 (Apr. 2019), pp. 256–260. DOI: 10.1126/science.aau0818.

[37] A. R. Its, B. -Q. Jin, and V. E. Korepin. *Entropy of XY Spin Chain and Block Toeplitz Determinants*. 2006. arXiv: quant-ph/0606178 [quant-ph].

[38] *NIST Digital Library of Mathematical Functions*. Release 1.1.9 of 2023-03-15. F. W. J. Olver, A. B. Olde Daalhuis, D. W. Lozier, B. I. Schneider, R. F. Boisvert, C. W. Clark, B. R. Miller, B. V. Saunders, H. S. Cohl, and M. A. McClain, eds. URL: https://dlmf.nist.gov/.

[39] Valentin Cré pel et al. "Universal signatures of Dirac fermions in entanglement and charge fluctuations". In: *Physical Review B* 103.23 (June 2021). DOI: 10.1103/physrevb.103.235108.

[40] I.S. Gradshteyn and I.M. Ryzhik. *Table of Integrals, Series, and Products*. Elsevier Science, 2014. ISBN: 9781483265643.